Rensselaer Polytechnic Institute

Troy, New York

PROGRESS REPORT
Covering Period from 15 March 1964
to 15 September 1964

RADIATION DAMAGE TO SEMICONDUCTORS BY HIGH-ENERGY ELECTRON AND PROTON RADIATION

John C. Corelli

Sponsored by the National Aeronautics and Space Administration

under Grant NsG-290

Department of Nuclear Engineering and Science
Rensselaer Polytechnic Institute
Troy, New York

Table of Content

I

Introduction and Summary

The results presented in this report were obtained in the radiation damage, research program sponsored by NASA (Grant NsG-290) during the period March 15, 1964 to September 15, 1964. During this period the following personnel were actively engaged in the research on a part time or full time basis.

Faculty:

Dr. John C. Corelli (full time)

Dr. H. B. Huntington* (part time, stopped June 10, 1964)

Graduate Students: (half time academic year - full time summer months)

Mr. Li-Jen Cheng

Mr. John F. Becker

Mr. John E. Fischer**

Mr. Orrin H. Merrill

Mr. Charles Taylor (left June 10, 1964)

Mr. Gordon Oehler (summer only 1964)

Mr. Arne Kalma

Research Technician: (full time)

Mr. James Westhead

Effective September 1, 1964 the Department of Nuclear Engineering and Science added two adjunct professors to its staff, Dr. James W. Corbett and Dr. George D. Watkins of the General Electric Research

---

* Other commitments dictate that Professor Huntington can no longer spend time as an active participant in the program. However, Professor Huntington will still consult with students on an informal basis as the occasion arises.

** AEC Fellow - salary charged to grant only during summer 1964.

Laboratory. Both Professor Corbett and Professor Watkins plan to be available for consultation in the program part time.

The general topics which are reported herein cover the following research: 1) Infrared studies on 36 and 60 Mev electron-irradiated pulled and floating-zone silicon and pulled germanium grown with varying oxygen content. The irradiations were carried out with the samples kept at a temperature of 320°K during bombardment, 2) electrical properties of Co^{60} photon* (1.25 Mev) and 15 and 45 Mev electron irradiation of germanium at 300°K, 3) carrier lifetime studies on germanium irradiated at 89°K by 48 Mev electrons, 4) low temperature (at 20°K) and cold temperature (at 80°K) irradiation of silicon and germanium with subsequent annealing studies to 350°K (electrical properties), 5) 1.5 Mev electron irradiation of silicon (at 300°K) and subsequent annealing to 800°K using carrier concentration and conductivity to detect the defects.

Portions of the results to be presented have appeared in various papers and presentations during the period March 15, 1964 - September 15, 1964 and are listed below.

1) "Studies of High-Energy Electron (10-60 Mev) and Proton (20-130 Mev) Radiation Damage in Silicon and Germanium". J. C. Corelli, Li-Jen Cheng, C. A. Taylor and O. H. Merrill. Paper given at 1964 International Conference on the Physics of Semiconductors, Symposium on Radiation Damage in Semiconductors, Paris, France, July 16-18, 1964. To be published

---

* Irradiated by John W. Cleland of Oak Ridge National Laboratory, Oak Ridge, Tennessee

in Proceedings.

2) Talks were given by Dr. J. C. Corelli, Li-Jen Cheng, O. H. Merrill, and J. F. Becker to the Instrument Research Group, Radiation Effects Section, NASA Langley Research Center, Hampton, Virginia, August 24 - 25, 1964. The content of the talks given are contained in this progress report.

3) "Role of Impurities in the 1.5 - 55 Mev Electron Irradiation of Silicon and Germanium." Seminar given by J. C. Corelli at the Aerospace Research Laboratory, Wright Patterson Air Force Base, Dayton, Ohio, September 11, 1964.

II

15-45 Mev Electron Irradiation of Germanium at 300°K*

Electron irradiation at 15 Mev and 45 Mev of initially 10 ohm-cm, n-type germanium (antimony and arsenic doped) of low dislocation content which had been previously irradiated with Co^{60} (1.25 Mev) photons was carried out. The electron irradiation was done in two steps, the first was a flux of about 5×10^{14} electrons/cm^2 on the samples and the second, about 5×10^{15} to 2×10^{16} electrons/cm^2 on the samples. The temperature dependence of the resistivity and carrier concentration was measured after each irradiation. The results in all cases are similar, so the graphs of one sample are sufficient to illustrate what happened. Figures 1 and 2 show the change during irradiation of the resistivity and Hall coefficient of Sb6#2, a 10 ohm-cm, antimony doped, n-type germanium sample. The break in Figure 1 is because the sample annealed (at 30°C) during the temperature measurements between irradiations. This is not evident on the Hall curve in Figure 2 as the slope is not large at that point. The resistivity initially increases but soon decreases and appears to approach a constant value. The Hall coefficient also increases a bit initially but then decreases, changes sign as the sample becomes p type, reaches a maximum, and then decreases toward an apparent constant value. Both initial increases are a transient effect possibly caused by dislocation migration or impurities. The maximum of the resistivity does not correspond with either the

---

* These experiments were conducted in cooperation with John W. Cleland of the Solid State Division at the Oak Ridge National Laboratory, Oak Ridge, Tennessee. The Co^{60} irradiation and the preparation of samples were performed by John W. Cleland.

point where the Hall coefficient changes sign or its maximum on either side. Figures 3 and 4 show the temperature dependence of the sample after successive irradiations. The sample was in an intrinsic condition after the Co^{60} photon irradiation and should have been p-type below room temperature. But it was n-type and probably had annealed before the first electron irradiation.

As control samples for the Co^{60} irradiated samples, some 30 ohm-cm germanium, both n-and p-type, and 14 and 1 ohm-cm p-type germanium (indium-doped) were also irradiated at the same energies to approximately the same fluxes and temperature dependence measurements were again taken. The 30 ohm-cm, n-type germanium samples had been previously irradiated with neutrons and annealed ($\approx$ 20 hrs. at 450°C) back to almost their initial condition. As before, the graphs for each type of sample are similar and only the results of one of each are shown. Figures 5 through 8 show the results for the 30 ohm-cm, p-type germanium. These samples were not avialable at the time of the first electron bombardment and thus there are no temperature dependence graphs after a small flux to ascertain if a steep slope, which was lessened by large fluxes, occurred there. Figures 10 and 11 are the temperature dependence of the n-type germanium. The irradiation measurements are almost exactly the same as those of the samples previously irradiated with photons and are not shown. Figures 12 through 15 show the results for the p-type, 14 ohm-cm germanium. Figures 16 and 17 are the temperature dependence graphs of the p-type, 1 ohm-cm germanium. Small changes were observed in conductivity at room temperature during the irradiation, so the irradiation curves are not included.

Some of the samples were observed to anneal after the irradiation was completed when left at room temperature. Figure 9 shows the time dependence of this annealing at $\approx 300^{\circ}K$ on the resistivity of one of the 30 ohm-cm, p-type germanium samples. Similar results were observed on other samples.

Temperature dependence runs were made on several types of samples which had previously been electron irradiated. The types of samples measured were: 10 ohm-cm, p-type, boron doped silicon and 10, 20, and 50 ohm-cm, n-type, antimony doped germanium. All of the germanium samples show an energy level in the range 0.20 - 0.26 ev below the conduction band and a deep unresolved level $\gtrsim 0.3$ ev below the bottom of the conduction band. The 50 ohm-cm material also shows an indication for a shallow level at about 0.1 ev below the conduction band.

In the following months, annealing experiments will be performed to determine at what temperature the defects anneal out.

III

Infrared Studies on 36 and 60 Mev Electron-Irradiated (at 320°K) Silicon and Germanium

Table I lists infrared samples which were irradiated during the period covered by this progress report. All samples were water cooled during irradiation and their temperature never exceeded 40°C. Spectra before and after irradiation were taken on two Perkin-Elmer spectrometers, the model 421 for covering the region between 2.5 and 15 microns, and the model 21 for the region between 0.7 and 2.5 microns. To obtain spectra with the samples at liquid nitrogen temperature, a cold cell with NaCl windows was used. Rectangular samples about 4 mm x 15 mm were held in the sample beam of the spectrometer by means of a clamping arrangment over a slit in a copper block which was in contact with liquid nitrogen.

The annealing was done in an electric furnace capable of reaching temperatures up to 600°C. A stainless steel basket was used to suspend the sample in silicon oil (up to 290°C) and air (300°C to 410°C). Several samples could be annealed at one time. All the samples annealed to date (numbers 1.1, 2.1, 3.1, 4.1, 5.2, 6.2, and 7.2) were annealed together isochronally.

Considerable data has been obtained from sample #7.2 (oxygen doped germanium). Prior to irradiation, the well-known intense absorption band due to the presence of oxygen in the sample was observed at 860 cm^{-1} (sample at 80°K). No other bands were detected in the region between 900 cm^{-1} and 600 cm^{-1}, after irradiation many other bands were observed in this region as shown in Figure 18.

Spectra after successive isochronal anneals (20 min. at each temperature in intervals of 10°C up to 290°C and 15°C from 300°C to 410°C) show growth and decay of the various bands (see Figures 18 and 19). After the 410°C anneal, all the radiation-induced defect absorption bands had disappeared. The relative defect concentration which was plotted vs. temperature of anneal in Figure 19 was obtained by measuring the area under each absorption peak. The bands shown for the oxygen doped germanium in Figure 18 are due to oxygen-defect complexes and are not found in germanium with low oxygen content.

The infrared properties of samples #5.2, 6.2 and 7.2 (germanium) were studied in the wavelength region between 1.8 and 8.0 microns. Absorption in this region has generally been associated with electronic excitation. Sample No. 5.2, which was p-type before irradiation, remained so after irradiation and through annealing. The spectrum of a p-type sample is typified by that of No. 5.2 shown in Figure 20. Samples 6.2 and 7.2 were n-type before irradiation and p-type after irradiation (determined from electrical properties). The shape of the spectrum of n-type germanium (pre-irradiation) is shown in Figures 21 and 22. The post-irradiation spectra of these samples is seen to be that characteristic of p-type germanium. Upon annealing, the spectra of these two are seen to return gradually to their pre-irradiation shape, indicating their return back to n-type conduction. The point where each sample returns to n-type is not exactly the same for these samples. Prior to irradiation they differed in resistivity by an order of magnitude, so that the large difference in impurity concentration strongly effects the annealing process (see section V of this

report for further results on the question of impurity effects in annealing). These infrared results seem to agree quite well with annealing experiments employing electrical measurements. Further annealing experiments are currently under way in our laboratory.

The silicon samples which were annealed isochronally up to 410°C with the germanium yielded basically the same results as those reported* earlier. Annealing has not been completed for the silicon samples, but is expected to be in the near future.

The irradiated silicon and germanium samples which have not been annealed will be used to study infrared properties using isothermal anneals with the aim of deducing activation energies.

---

* A report covering the details of this work was submitted to NASA September 17, 1964 and will not be repeated here. The title of the report is "Annealing of Infrared Defect Absorption Bands in 40 Mev Electron-Irradiated Silicon" by J. C. Corelli, G. Oehler, J. F. Becker and K. J. Eisentraut.

IV

Carrier Lifetime Studies on Germanium Irradiated at 89°K by 48 Mev Electrons

One low-temperature irradiation was performed, primarily to check out experimental equipment and procedures. A large sample (1/4" x 1/4" x 3/4") of 4 ohm-cm indium-doped germanium was irradiated at 89°K with about 10^{12} electrons/cm^2 of 48 Mev. This dose was sufficient to reduce the filament lifetime at 89°K from 27μ sec to 2.8μ sec. Lifetime was measured by observing the decay of photoconductivity induced by unfiltered light from a xenon flashtube, with which an injection level of 10% was achieved at the lowest temperature and maintained constant throughout the experiment. Surface effects were minimized by using a large, well-prepared sample and by waiting until half the excess carriers decayed before making measurements. A similar sample was irradiated at room temperature to about 1/3 the above dose, causing the room temperature lifetime to go from 230μ sec to 42μ sec.

The results of the first 10 minute isochronal annealing experiment shown in Figure 23, are to be considered very tentative. The increase in recombination center density at $\sim$140°K is similar to observations in silicon using electrical properties to detect defects, and is probably due to migration of primary defects into a more stable center which has a larger capture cross-section than the primary defect. It is significant to note that the predominant annealing at $\approx$170°K is in the same temperature region as occurs for carrier concentration annealing in p-type germanium of comparable

resistivity (see previous progress report covering period 15 March 1964 - 15 September 1964, p. 9). This experimental result suggests that the carrier trap and the recombination center may be associated with the same defect. Further experiments in this area are currently in progress.

Figure 24 shows the temperature dependence of lifetime before irradiation and after the last anneal (330°K). At temperatures below 1000/T = 4, the rate-limiting process is thermal excitation of majority carriers both before and after irradiation; the slopes shown probably correspond to acceptor levels. The number of recombination centers is proportional to $1/\tau$, so although most of the "damage" has been annealed at 330°K or lower, the lifetime is still about 1/3 the pre-irradiation value.

This experiment demonstrated the severity of the inherent limitations of the pulsed light source. The pulse is too wide in time to allow introduction of large numbers of defects. Most of the energy output is in the visible portion of the spectrum and hence is absorbed near or at the sample surface. The light is not intense enough to allow use of a germanium filter at low temperatures or with low-resistivity material. One cannot perform injection-level dependence studies at low temperatures (to study cross-sections). It is hoped that all of these difficulties will be surmounted by using a pulsed 75 KVP x-ray tube which has recently been procured* and which should be operational by December 1964.

---

*This equipment was given to us by the X-Ray Department of the General Electric Company, and we acknowledge their generous gift.

V

Low Temperature (20°K) and Cold Temperature (80°K) Irradiation and Annealing of 45 Mev Electron-Irradiated Silicon and Germanium

A) Recovery of 47 Mev Electron-Induced Defects in N-Type Ge from 20°K to 288°K

One sample of Sb-doped 0.2 Ω-cm Ge was irradiated with 47 Mev electrons at a temperature below 20°K. The total flux of the electrons incident on the sample was 3.12×10^{14} e/cm^2. A 10-minute isochronal annealing experiment up to the temperature of 288°K was performed. There were four annealing peaks found located at about 36°K, 65°K, 130°K, and 205°K (Figure 25). The first two recovery stages would be considered to correspond to the stages found by Mackay and Klontz[1] in the study of 1.10 Mev electron-irradiated Ge at low temperature. The two other peaks may belong to the annealing of the defects produced by high energy electrons only, since there has not been any annealing reported on low energy (0.5 Mev) electron-irradiated N-type Ge at those temperatures[2]. However, further experiments will be performed to study this point in more detail.

One sample of As-doped 3.5 Ω-cm n-type Ge was irradiated at 80°K by 45 Mev electrons to a total flux of 6.4×10^{13} e/cm^2 and isochronally annealed for 10 minutes up to 338°K. Two annealing

processes similar to the 130°K and 205°K peaks shown in Figure 25 were found in the measurement of conductivity.

One isothermal annealing experiment at 185°K was performed on a 45 Mev electron-irradiated 10Ω-cm arsenic doped Ge sample. For this sample, we have plotted $\frac{1}{\mu_H}$ vs. $\frac{1}{R_H}$ in Figure 26 (R_H is the Hall coefficient, μ_H is the Hall mobility). The two distinct slopes indicate that at least two kinds of defects (or different charge states of the same defect) anneal out at the temperature 185°K. The kinetics corresponding to the annealing of the defects disappearing faster is found to be second-order.

B) Recovery of 54 Mev Electron-Induced Defects in P-Type Ge from 20°K to 300°K.

One sample of In-doped 0.7Ω-cm was irradiated with 54 Mev electrons at a temperature below 20°K. The total electron flux was 2.5×10^{14} e/cm^2. The carrier removed rate was about 0.0004 $\frac{h}{e\text{-}cm}$, but this did not mean that the damage was very small, since the change of the mobility was rather large and the total number of carriers removed was also large, which was ascertained after the sample was warmed up to 90°K and measured at that temperature. A 10-minute isochronal annealing experiment was performed. The data corresponding to the annealing temperature range from 20°K to 90°K were rather scattered, since they were measured at 13°K where the temperature dependences of the Hall coefficient and the resistivity were too strong to be measured accurately at a constant reference temperature. The data for the annealing experiment at temperatures from 90°K to 300°K are

shown in Figure 27. The increases of the resistivity and the Hall coefficient below 160°K were observed after each annealing, which was considered as unloading the trapped minority carriers from defects located below the edge of the conduction band. After the sample was irradiated with white light at the temperature of about 80°K, the resistivity and the Hall coefficient decreased and the mobility increased (see Figure 28). This should correspond to loading of traps. The lifetime of the electron trapped was extremely long, the order of days at least. The defect centers participating in the trapping effect must have a charge of at least +2 before capturing an electron, otherwise the hole capture cross section would not be so small.

A recovery stage was found at the temperature of about 180°K, which should correspond to the annealing of the defects responsible for the trapping effect mentioned above, since there was no trapping effect observed after the recovery stage.

C) Recovery of 45 Mev Electron-Induced Defects in N-Type Silicon from 80°K to 360°K.

Several single crystalline samples of phosphorous-doped silicon were irradiated with 45 Mev electrons at the temperature of about 80°K, and then isochronally annealed 10 minutes at each temperature from 80°K to 360°K. In all the cases, the result shows that there is a distinct difference in the recovery behavior of the damage between the pulled crystal samples and floating-zone samples. A typical example is shown in Figure 29, in which the fractions of damage remaining in carrier concentrations of three samples with almost the same resistivities (10 - 11 Ω-cm) were

plotted verses the annealing temperature. There were some increases in the defect concentration of the samples at 78°K after the irradiations stopped. The amount of the increase depends on the total dose received by the sample. It may be due to some irradiation-induced defects unstable at that temperature, or some slow carrier trapping effect. Some further experiments are needed in order to make this point clear.

Three recovery stages are observed in the 10 Ω-cm floating-zone crystals located at about 125°K, 190°K, and 260°K. The pulled crystals exhibited three other annealing processes, located at about 100-200°K, 240°K, and 290°K. Similar annealing behavior was observed on 1 Ω-cm pulled crystal sample of P-doped silicon. The annealing process at 100-200°K is rather broad, and might be due to an overlapping of two or more recovery stages. The recovery stages at 125° and 190°K in the two floating-zone samples were found to be dose dependent. An annealing experiment of one 1 Ω-cm floating-zone sample irradiated with much higher dose (1.4×10^{15} e/cm^2) showed only a broad recovery stage from 100 to 220°K which supports the interpretation of the dose dependence.

The recovery stage at 240°K appears as a small reverse annealing process (see Figure 29), not a carrier trapping effect. This was determined by using a method of illuminating with white light at 78°K to investigate for the presence of traps. The recovery stage at 290°K in the pulled crystals was a main annealing process in which about one-fifth of the total defect concentration was annealed out in the 11 Ω-cm sample. The two annealings at 240°K and 290° appear to be characteristic of defects associated with

oxygen atoms, since they do not occur in floating zone silicon containing less dispersed oxygen.

In general the amount of defects annealed out (in carrier concentration) in the pulled crystals appears to be higher than that in the floating-zone crystals in the temperature range 80-360°K. The fractions of damage annealed out in carrier concentration up to 360°K in pulled and in floating-zone crystals are about 55% and 32% respectively. In Figures 30 and 31, the reciprocal Hall mobilities were plotted verses the carrier concentrations. The results show that the annealing curve is very close to the irradiation curve for the pulled crystal, but this is not the case for the floating-zone sample in which the mobility anneals with a faster rate at lower temperatures, and also the annealing processes in the latter seem to be more complicated.

The temperature dependence of the carrier concentrations of one floating-zone sample and one pulled crystal were plotted in Figures 32 and 33 respectively. There were about 70% of the defects remaining after 354°K annealing belonging to the oxygen-vacancy complex (A-center) in the pulled crystal sample of 11 Ω-cm. The fraction of the defects remaining which would correspond to A-centers was lower in the pulled crystal 1 Ω-cm sample.

The difference between the pulled crystal and the floating-zone crystal may be interpreted as follows; the oxygen concentration in the pulled crystal is very high, about 10^{17} - 10^{18} atoms/cc, the defects associated with oxygen atoms should be dominant; in the

floating-zone crystal, other imperfections (such as other impurities, dislocations) should be dominant, therefore the defects produced should be different and possibly more complex than in the pulled crystal silicon.

In conclusion, we may say that the formation and the annealing (from 80° to 360°K) of defects under 45 Mev electron irradiation at about 80°K strongly depend on the types and the concentrations of the imperfections originally existing in the sample, such as oxygen. They also depend on the total dose. In order to understand the mechanism of the formation and the annealing of the irradiation-induced defects more clearly, additional methods of microscopic measurement are needed, such as spin resonance, photo-conductivity, and infrared absorptivity.

VI

1.5 Mev Electron Irradiation (300°K) of N-Type Silicon and Annealing Studies to 800°K

The samples listed in Table II were irradiated at the General Electric Research Laboratory's resonant transformer accelerator. The accelerator was operated at an electron energy 1.5 Mev, and at an average current of 400 μa. Samples Si-P(0) and 114 H-2 received 1.34×10^{16} e/cm^2 and samples F1-99 and 152-2 received 2.68×10^{16} e/cm^2, all four at a rate of 1.9×10^{13} e/cm^2 sec.

A plot of $\frac{\rho-\rho_0}{\rho_0}$ vs. ϕ t revealed that: (1) the removal rates are not strikingly non-linear, with a small ($\approx$30%) difference between initial and final removal rates, (2) the room temperature removal rate was down a factor of four for pulled silicon compared to FZ silicon.

The energy of the levels introduced was measured following a method reported in Kitovskii et al[3]. Table III lists the energy levels for each sample. A defect energy level at E_c-0.17ev was not introduced in sample 152-2 in sufficient quantity to be measured. The minima listed for the deep levels were established on the basis of Fermi level calculations. A low enough temperature was not reached to produce a straight line for the shallow levels on a ln(n) vs. 1000/T plot. The values listed are minimum values.

Table IV lists the number of electrons in each level at T=0°K. These numbers were obtained by subtracting successive complete ionizations as indicated by the lightly dashed lines in Figures 34 - 37. The number of deep levels introduced is somewhat

difficult to establish because of the temperature dependence of the ratio of Hall to drift mobility which causes the apparent carrier concentration to drop off at temperatures above 200°K in the unirradiated silicon.

Annealing of sample Si-P(0) was carried out with 20 minute anneals every 20° to 25°C up to 400°C, and then in larger steps to 534°C. The number of A-centers vs. annealing temperature is shown in Figure 38. The predominate annealing takes place between 240° and 400°C, with 50% remaining at 320°C. This compares well with the A-center annealing reported elsewhere[4]. Infrared measurements with 40-50 Mev electron-irradiated silicon performed at R.P.I. show that the annealing of the A-center, 12 μ (834 cm^{-1}) band correlates well with the annealing in this experiment, except the 12 μ anneal is initiated at a higher temperature. This is due most probably to a) the growth which competes with annealing and shifts the beginning of the anneal to a higher temperature and b) the higher purity of the samples in the infrared work.

A-center growth, reported by Tanaka and Inuishi[5], and also in the IR work cited above, was small ($<5\%$) with this sample.

The annealing characteristics of the deep levels are shown in Figure 39. Two definite stages are present, one centered at 140°C, and the other at 360°C. The first is most probably the E-center which other workers[4,6] have found to be ≈ 0.4 ev below the conduction band. The annealing temperatures agree with those found elsewhere[4,5,7]. The second stage, which has not previously been observed with electrical property measurements, to our

knowledge, has been suggested as possibly being associated with the divacancy[4]. The number introduced, however, seems rather high for the production of divacancies[8]. On the basis of the annealing data, we find that the first stage (E-center) has been introduced at a rate of ~.03/elec.cm, and the second stage (divacancy?) at a rate of ~.04/elec.cm. The carrier concentration at 300°K is very stable after the second annealing stage up to 530°C.

The data indicate that a new shallow level has been introduced at approximately 250°C which has disappeared after anneal to 370°C. Above 390°C, some more complex behavior sets in which indicates the creation of another level which is gone by 530°C. The first growth and decay (250°-270°C) is not correlated to any observed IR band. The second (390°-530°C) correlates with the 394 cm^{-1} (11.2 μ) band (350°-550°C).

Difficulty in low temperature measurements (caused by the thermocouple bead's not being in contact with the sample makes quantitative analysis of the growth and energy of the new levels difficult. It might be easier to make such measurements by longer irradiations of oxygen containing silicon, which could be annealed at 300°C for a long time. This would serve to remove the A-centers which tend to mask any nearby levels. Such a method might make possible a measurement of the energy of the level, as well as its annealing characteristics.

TABLE I

Sample No.	Type and Impurity	Initial* Resistivity	Crystal Growing Method	Incident Energy (Mev)	Total Integrated Flux X 10^{-18} e/cm^2	Thickness (mm)
1.1, 1.2	p-Type Si Boron	100 Ω-cm	Pulled Crystal	60	2.5, 1.2	6.33
2.1, 2.2	n-Type Si Phosphorous	100 Ω-cm	Pulled	60	2.5, 1.2	5.26
3.1	n-Type Si Phosphorous	1.0 Ω-cm	FZ	60	1.3	5.97
4.1	n-Type Si Phosphorous	0.1 Ω-cm	FZ	60	1.3	5.30
5.1, 5.2	p-Type Ge Indium	0.1 Ω-cm	Pulled	36	6.9, 5.6	4.24
6.1, 6.2	n-Type Ge Sb	0.1 Ω-cm	Pulled	36	6.9, 2.8	4.34
7.1, 7.2, 7.3	n-Type Ge Oxygen**	1.0 Ω-cm	Pulled	57	2.1, 3.3, 1.3	6.57, 6.55, 6.58

* pre-irradiation value @ 300^{o}K

** grown in oxygen atmosphere

TABLE II

Pre-Irradiation Sample Characteristics

Sample No. and Growth Method	Impurity	Carrier Concentration* $\frac{\text{atoms}}{\text{cm}^3}$	Resistivity* (ohm-cm)	Mobility* $\frac{\text{cm}^2}{\text{volt-sec}}$	Thickness (inches)
Si-P(O) (Pulled)	P	4×10^{15}	1.2	1350	.025
114 H-2 (F.Z.)	P	6×10^{15}	.70	1500	.027
152-2 (F.Z.)	As	13×10^{15}	.41	1200	.030
1-99 (F.Z.)	Sb	16×10^{15}	.44	900	.051

* Measured at $300^{\circ}K$

TABLE III

Position of Energy Levels After Irradiation (E_C-E_D)

Sample No.	Shallow*	Intermediate	Deep***
Si-P(O)	.034	.170 ± .005	.30
114 H-2	.034	.18 ± .02	.32
152-2	.040	**	.30
1-99	.027	.17 ± .02	.30

* These are minimum values. (See text)

** Insufficient quantity to measure.

*** Based on Fermi Level.

TABLE IV

Number of Electrons Trapped at $0^{o}K$/elec cm.

Sample No.	Shallow	.17 ev	Deep	Dose
Si-P(O)	.048	.186	.11*	1.34×10^{16} e/cm^2
114 H-2	.030	.059	.45*	1.34×10^{16} e/cm^2
152-2	.056	.03	.44*	2.68×10^{16} e/cm^2
1-99	.074	.074	.52*	2.68×10^{16} e/cm^2

* Approximate, because of μ_H/μ temperature dependence. (See text)

References

1. J. W. Mackay and E. E. Klontz, J. Appl. Phy. 30, 1269 (1959).
2. W. L. Brown, W. M. Augustyniak, and T. R. Waite, J. Appl. Phys. 30, 1258 (1959).
3. N. A. Kitovskii, T. V. Mashovets, and S. M. Ryvkin, Soviet Physics - Solid State 4, 2088 (1963).
4. E. Sonder and L. C. Templeton, J. Appl. Phys. 34, 3295 (1963)
5. T. Tanaka and Y. Inuishi, J. Phys. Soc. Japan 19, 167 (1964)
6. G. D. Watkins, J. W. Corbett, and R. M. Walker, J. Appl. Phys. 30, 1198 (1959).
7. H. Saito, M. Hirata, and T. Horivchi, Proc. Int. Conf. Latt. Def. J. Phys. Soc. Japan 18 Suppl.III, 246 (1963).
8. J. W. Corbett and G. D. Watkins, Phys. Rev. Letters 7, 314 (1961).

List of Figures

Fig. 11 Carrier concentration vs. 1000/T(^{o}K) for 30 Ω-cm antimony-doped germanium after bombardment by 55 and 46 Mev electrons at 300^{o}K.

Fig. 12 Resistivity vs. total flux for 14 Ω-cm p-type germanium (indium-doped) bombarded by 46 Mev electrons at 300^{o}K.

Fig. 13 Carrier concentration vs. total flux for 14 Ω-cm p-type germanium (indium-doped) bombarded by 46 Mev electrons at 300^{o}K.

Fig. 14 Resistivity vs. 1000/T(^{o}K) for 14 Ω-cm p-type germanium (indium-doped) before and after 46 Mev electron bombardment at 300^{o}K.

Fig. 15 Carrier concentration vs. 1000/T(^{o}K) for 14 Ω-cm p-type germanium (indium-doped) before and after 46 Mev electron bombardment at 300^{o}K.

Fig. 16 Resistivity vs. 1000/T(^{o}K) of $\approx$2 Ω-cm p-type germanium (indium-doped) after 11.8 and 17 Mev electron bombardment at 300^{o}K.

Fig. 17 Carrier concentration vs. 1000/T(^{o}K) of $\approx$2 Ω-cm p-type germanium (indium-doped) after 11.8 and 17 Mev electron bombardment at 300^{o}K.

Fig. 18 Infrared spectra of 57 Mev electron-irradiated (320^{o}K) oxygen-doped germanium after 20 minute anneals at various temperatures from 70^{o}C to 410^{o}C.

Fig. 19 Isochronal anneals (20 minutes at each temperature) of defect absorption bands induced in n-type oxygen-doped germanium by 57 Mev electrons (320^{o}K).

Fig. 20 Infrared spectra (1-8 microns) of 0.1 Ω-cm indium-doped germanium before irradiation and after 36 Mev electron irradiation (320°K) and twenty minute annealing at temperatures from 118°C to 251°C.

Fig. 21 Infrared spectra (1-8 microns) of 0.1 Ω-cm antimony-doped germanium before irradiation and after 36 Mev electron irradiation (320°K) and twenty minute annealing at temperatures from 70°C to 280°C.

Fig. 22 Infrared spectra (1-8 microns) of 1 Ω-cm n-type oxygen-doped germanium before irradiation and after 57 Mev electron irradiation (320°K) and twenty minute annealing at temperatures from 144°C to 323°C.

Fig. 23 Fraction of damage remaining in carrier lifetime, f, vs. annealing temperature (10 minute anneals) after 48 Mev electron irradiation of 4 Ω-cm indium-doped germanium at 90°K.

$f = \frac{1/\tau - 1/\tau_o}{1/\tau_b - 1/\tau_o}$ where τ_o is the pre-irradiation lifetime, τ_b is the post-irradiation lifetime and τ is the lifetime following an anneal at temperature T. All measurements of f made at 90°K.

Fig. 24 Temperature dependence of lifetime for 4 Ω-cm indium-doped germanium before irradiation and after irradiation by 48 Mev electrons at 90°K and anneal at 330°K.

Fig. 25 Fraction of damage remaining $\frac{\Delta n}{\Delta n_o}$ vs. annealing temperatures for 10 minute isochronal anneals of 0.2 Ω-cm antimony-doped germanium bombarded by 47 Mev electrons at 20°K.

Fig. 26 $\frac{1}{\mu_H}$ vs. $\frac{1}{R_H}$ for 185°K isothermal anneal of 10 Ω-cm arsenic-doped germanium bombarded by 46 Mev electrons at 93°K.

Fig. 27 Hall coefficient and resistivity curves of 10 minute isochronal anneals from 90°K to 300°K for 0.7 Ω-cm indium-doped germanium irradiated with 45 Mev electrons at 20°K.

Fig. 28 Loading the minority carrier traps with white light at 90°K in the 0.7 Ω-cm indium-doped germanium irradiated with 45 Mev electrons at 20°K.

Fig. 29 Fraction of damage remaining $\frac{\Delta n}{\Delta n_o}$ vs. annealing temperatures for 10 minute isochronal annealing of three phosphorous-doped silicon samples irradiated with 44-45 Mev electrons at 80°K.

Fig. 30 $\frac{1}{\mu_H}$ vs. n for irradiation and 10 minute isochronal anneals of 10 Ω-cm phosphorous-doped floating-zone silicon.

Fig. 31 $\frac{1}{\mu_H}$ vs. n for irradiation and 10 minute isochronal anneals of 11 Ω-cm phosphorous-doped pulled-crystal silicon.

Fig. 32 Temperature dependence of carrier concentration of irradiated 10 Ω-cm phosphorous-doped floating-zone silicon after various temperature anneals.

Fig. 33 Temperature dependence of carrier concentration of irradiated 11 Ω-cm phosphorous-doped pulled-crystal silicon after various temperature anneals.

Fig. 34 Carrier concentration vs. 1000/T for 0.7 Ω-cm phosphorous-doped floating-zone silicon before and after irradiation by 1.5 Mev electrons at 320°K.

Fig. 35 Carrier concentration vs. 1000/T for 0.4 Ω-cm arsenic-doped floating-zone silicon before and after irradiation by 1.5 Mev electrons at 320°K.

Fig. 36 Carrier concentration vs. 1000/T for 0.4 Ω-cm antimony-doped floating-zone silicon before and after irradiation by 1.5 Mev electrons at 320°K.

Fig. 37 Carrier concentration vs. 1000/T for 1.2 Ω-cm phosphorous-doped pulled silicon before and after irradiation by 1.5 Mev electrons at 320°K. Also shown are temperature dependences after 20 minute anneals at temperatures from 125°C to 534°C.

Fig. 38 Number of Si-A centers vs. annealing temperature (20 minute anneals) for 1.2 Ω-cm phosphorous-doped pulled silicon after 1.5 Mev electron irradiation at 320°K.

Fig. 39 Number of deep levels vs. annealing temperature (20 minute anneals) for 1.2 Ω-cm phosphorous-doped pulled silicon after 1.5 Mev electron irradiation at 320°K.

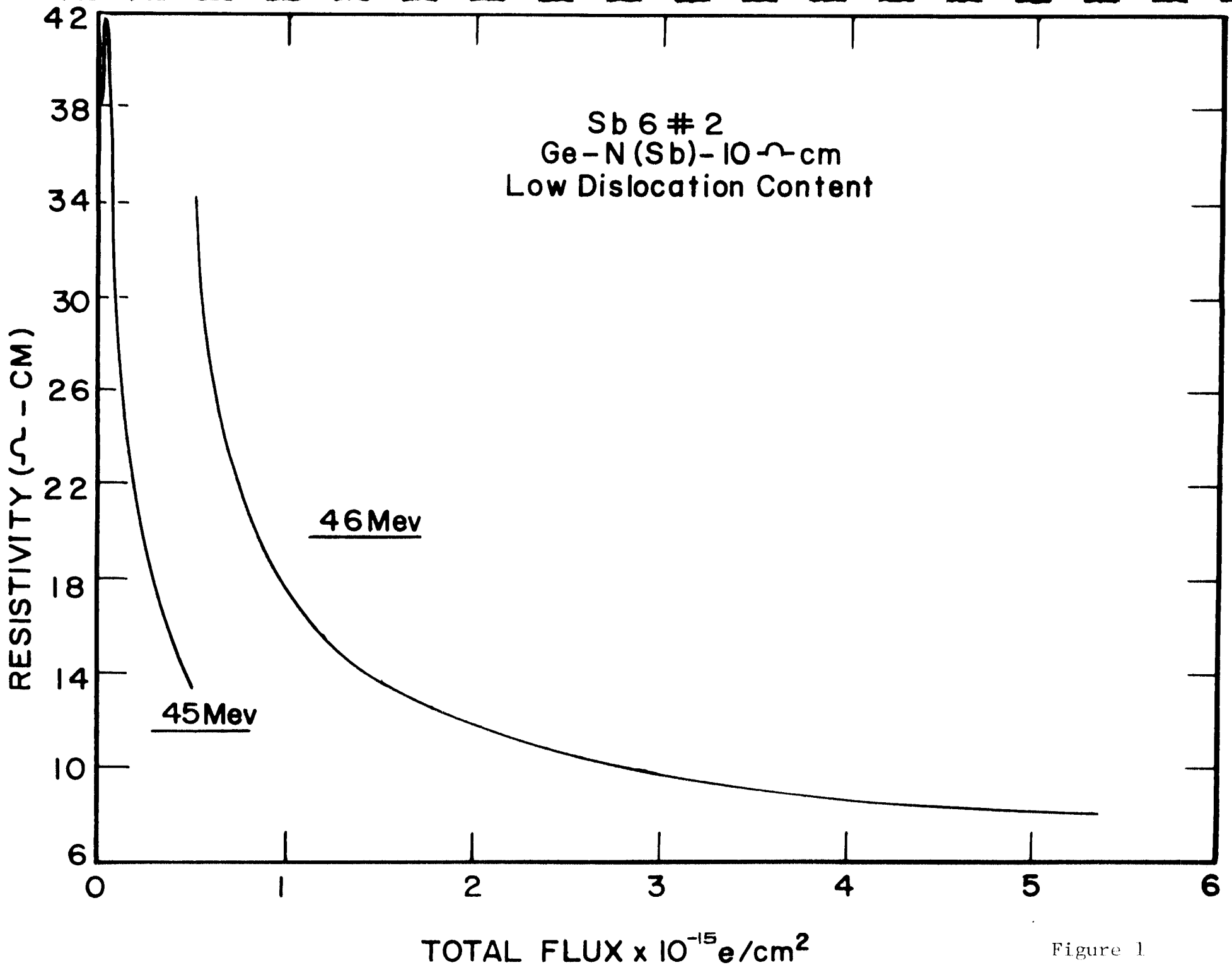
Sb 6 # 2
Ge – N (Sb) – 10 Ω-cm
Low Dislocation Content
46Mev
45Mev
RESISTIVITY (Ω – CM)
42
38
34
30
26
22
18
14
10
6
0
1
2
3
4
5
6
TOTAL FLUX x 10^{-15} e/cm^2

Figure 1

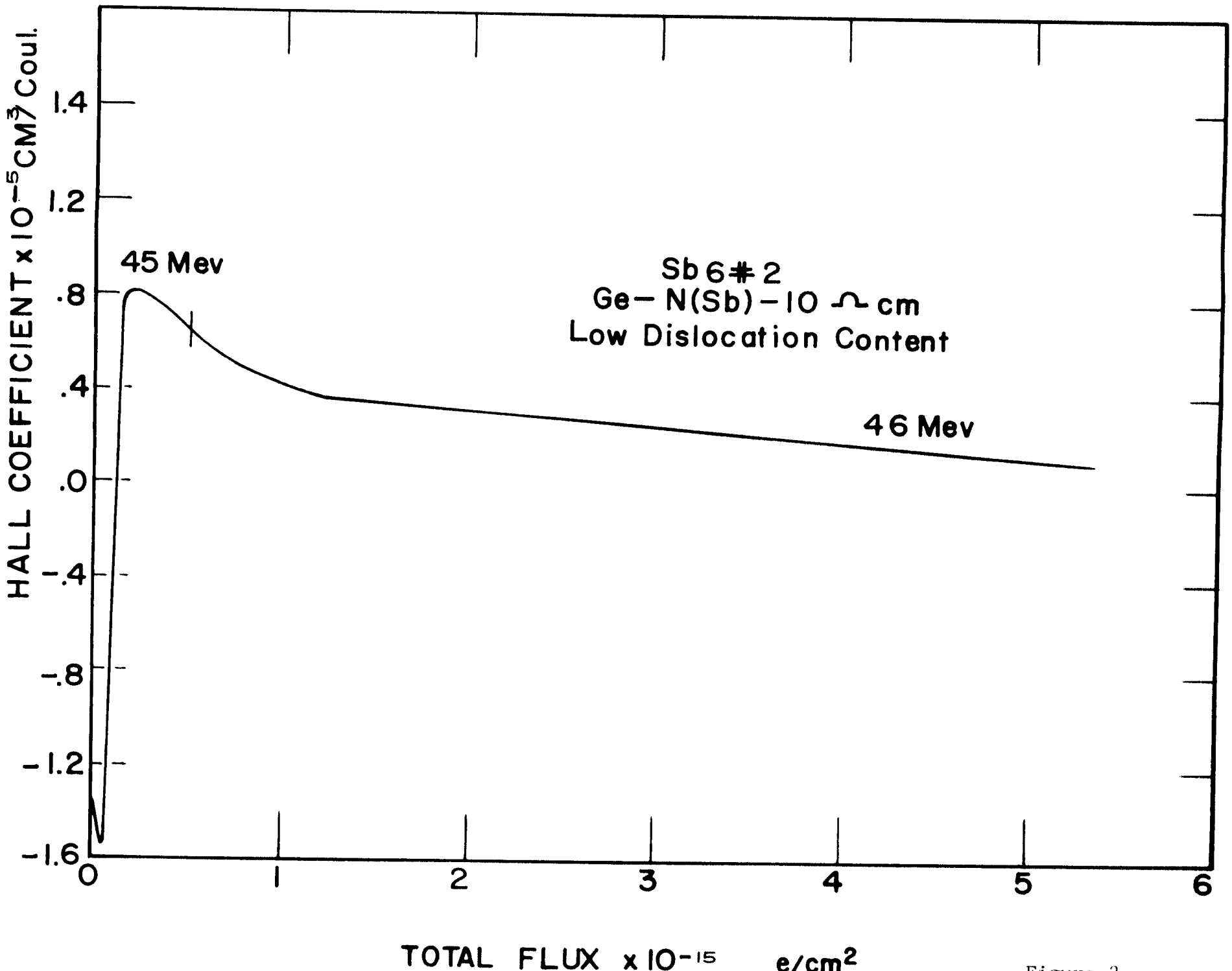
HALL COEFFICIENT x 10⁻⁵ CM³/ Coul.
1.4
1.2
.8
.4
.0
-.4
-.8
-1.2
-1.6
0
1
2
3
4
5
6
45 Mev
Sb 6 # 2
Ge – N(Sb) – 10 Ω cm
Low Dislocation Content
46 Mev
TOTAL FLUX x 10⁻¹⁵ e/cm²

Figure 2

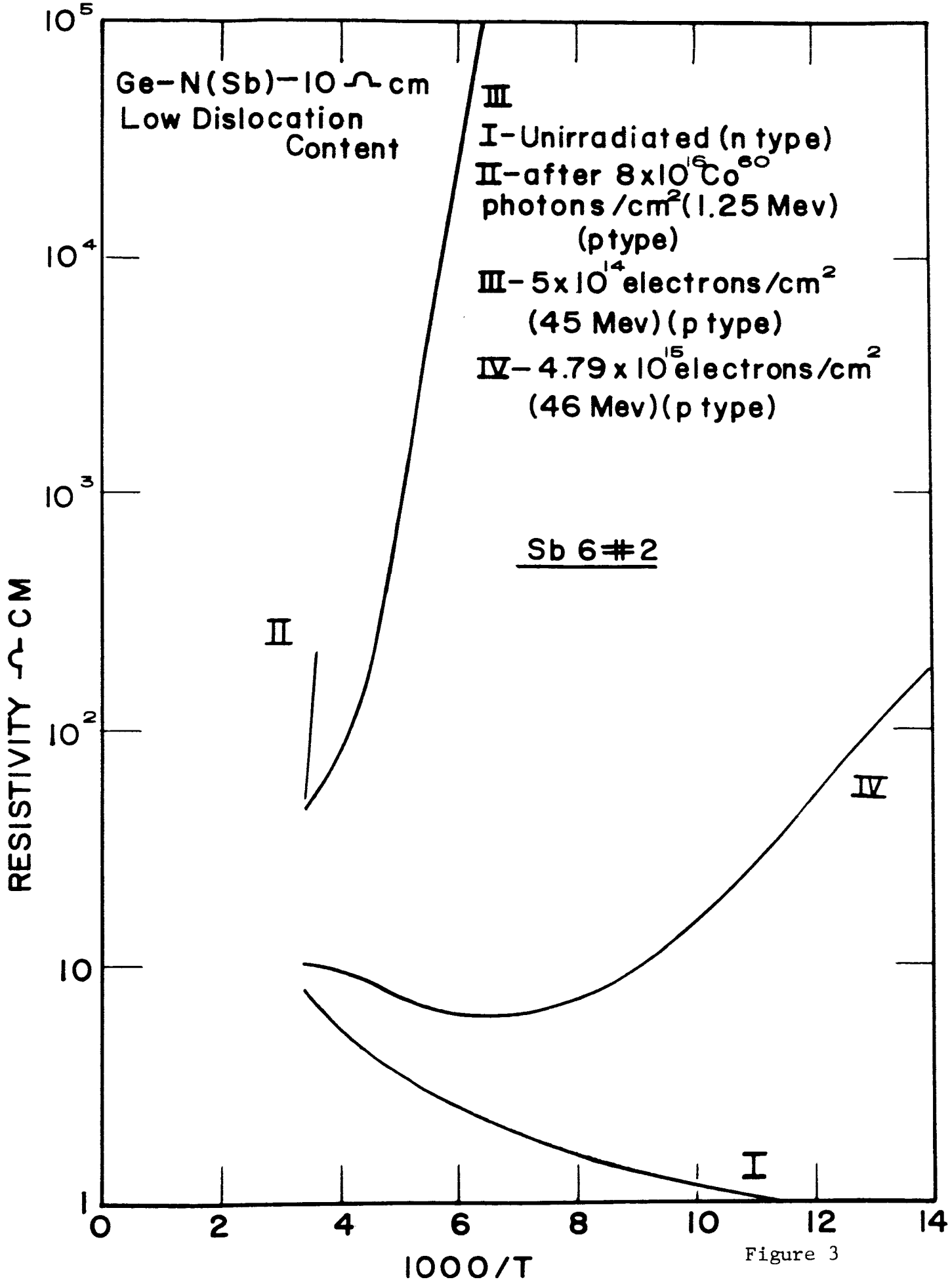
Ge-N(Sb)-10 Ω-cm
Low Dislocation
Content
III
I-Unirradiated (n type)
II-after 8x10^16 Co^60
photons/cm^2 (1.25 Mev)
(p type)
III-5x10^14 electrons/cm^2
(45 Mev) (p type)
IV-4.79x10^15 electrons/cm^2
(46 Mev) (p type)
Sb 6#2
II
IV
I
RESISTIVITY Ω-CM
10^5
10^4
10^3
10^2
10
1
0
2
4
6
8
10
12
14
1000/T

Figure 3

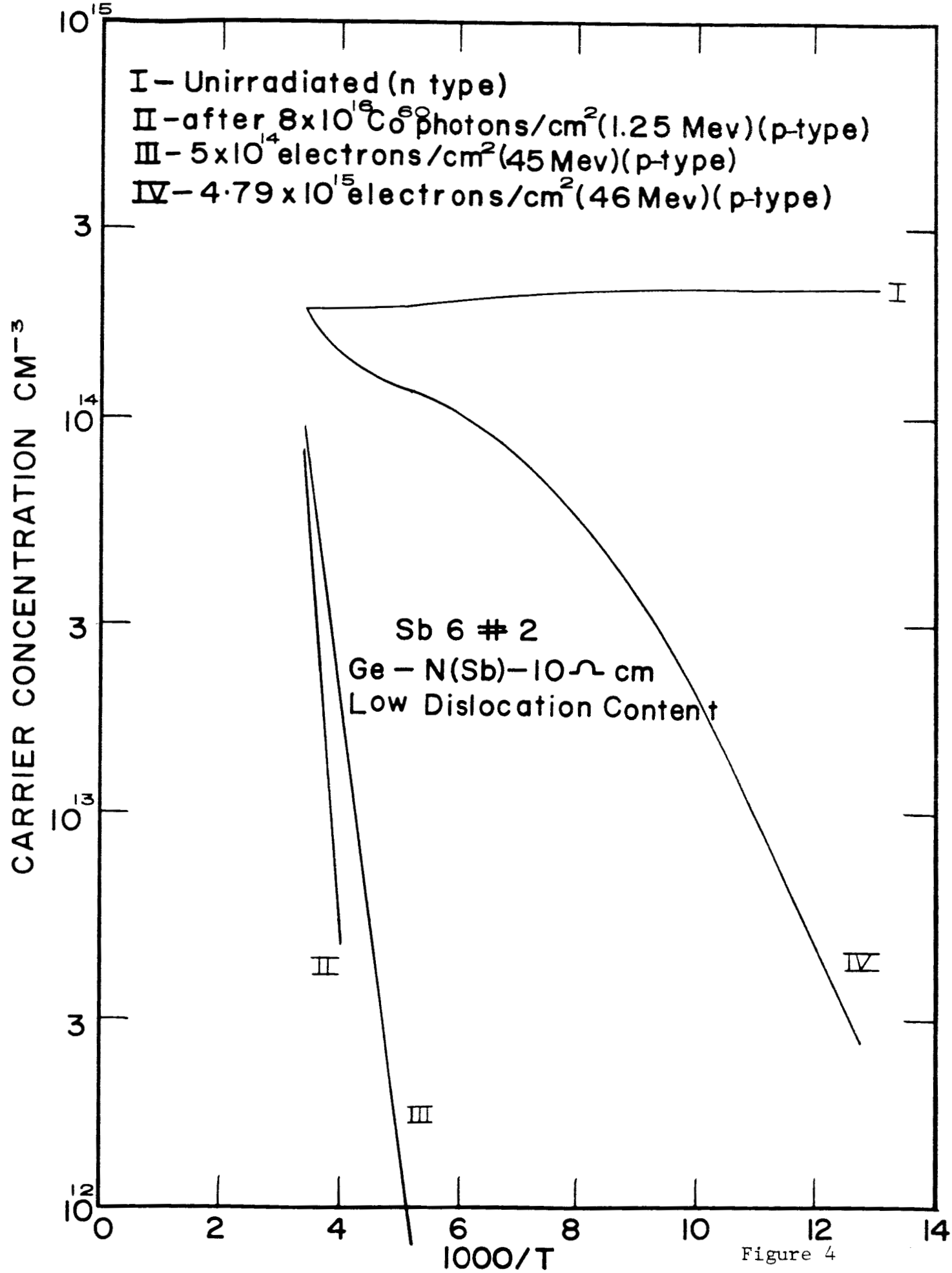
I – Unirradiated (n type)
II – after 8x10^16 Co^60 photons/cm^2 (1.25 Mev) (p-type)
III – 5x10^14 electrons/cm^2 (45 Mev) (p-type)
IV – 4·79x10^15 electrons/cm^2 (46 Mev) (p-type)
Sb 6 # 2
Ge – N(Sb) – 10 Ω cm
Low Dislocation Content
CARRIER CONCENTRATION CM^-3
1000/T
10^15
3
10^14
3
10^13
3
10^12
0
2
4
6
8
10
12
14
I
II
III
IV

Figure 4

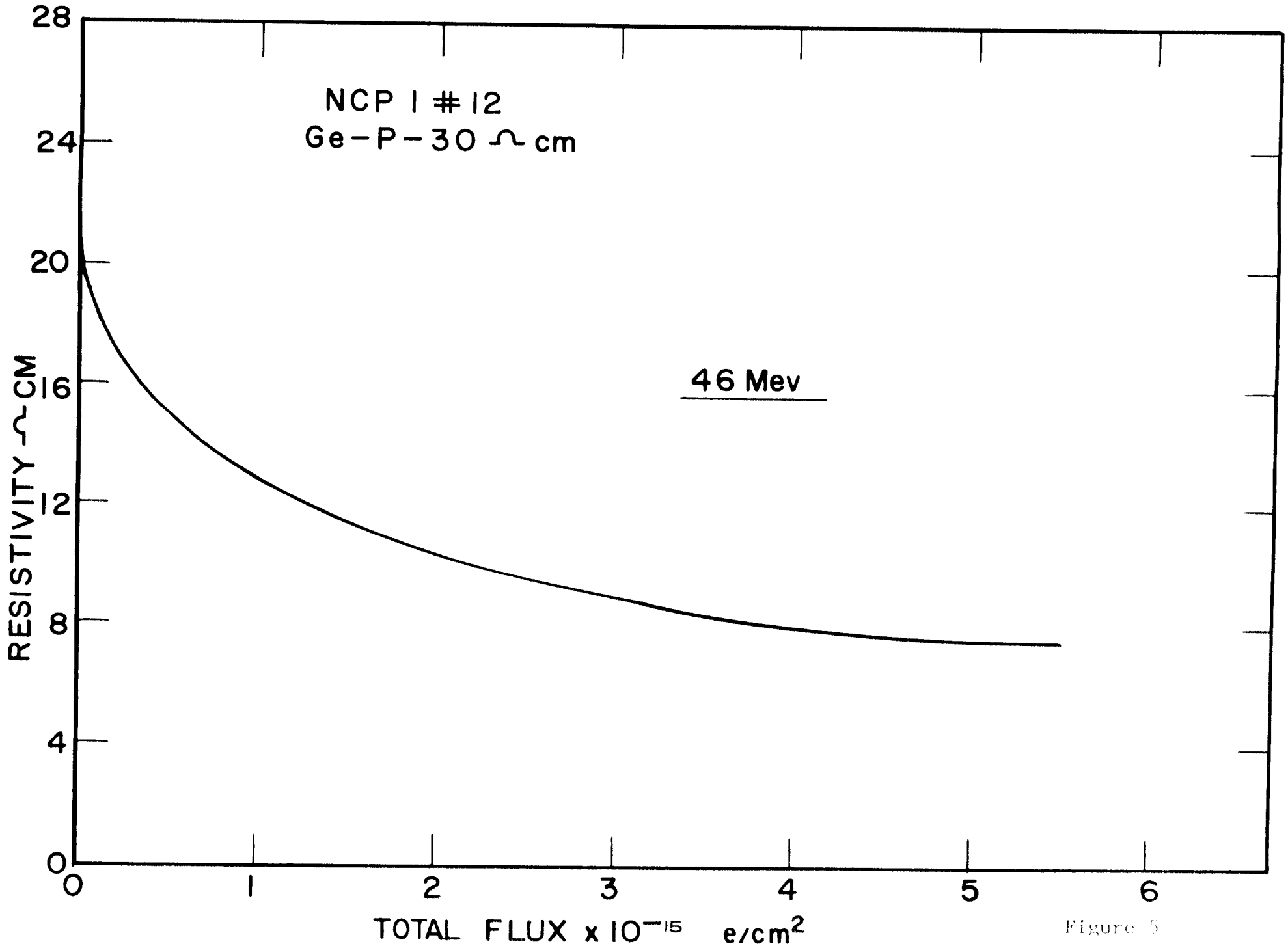
NCP 1 #12
Ge-P-30 Ω cm
46 Mev
RESISTIVITY Ω-CM
TOTAL FLUX x 10⁻¹⁵ e/cm²
0
4
8
12
16
20
24
28
0
1
2
3
4
5
6

Figure 5

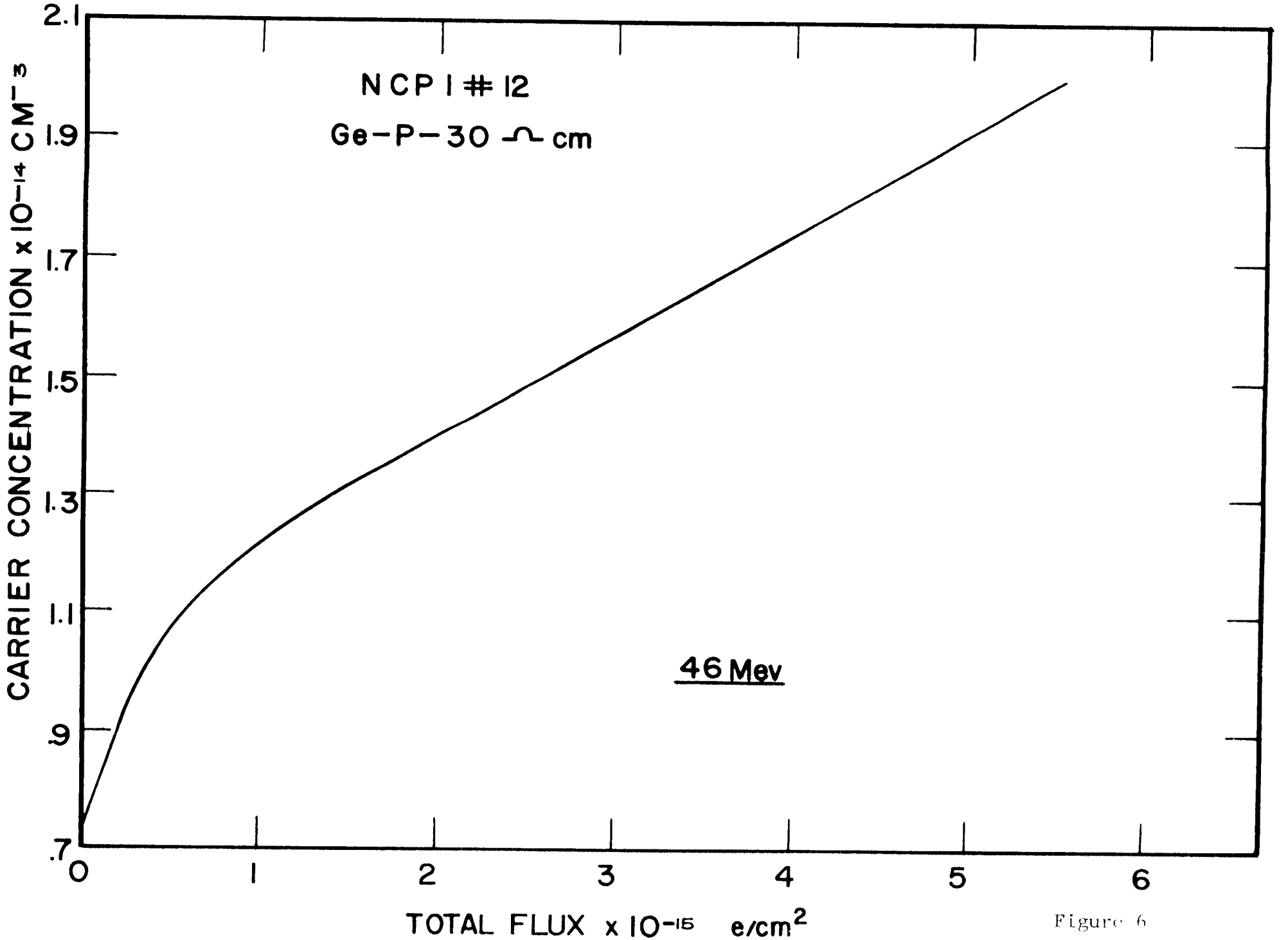
NCP I # 12
Ge-P-30 Ω-cm
46 Mev
CARRIER CONCENTRATION x 10⁻¹⁴ CM⁻³
TOTAL FLUX x 10⁻¹⁵ e/cm²
2.1
1.9
1.7
1.5
1.3
1.1
.9
.7
0
1
2
3
4
5
6

Figure 6

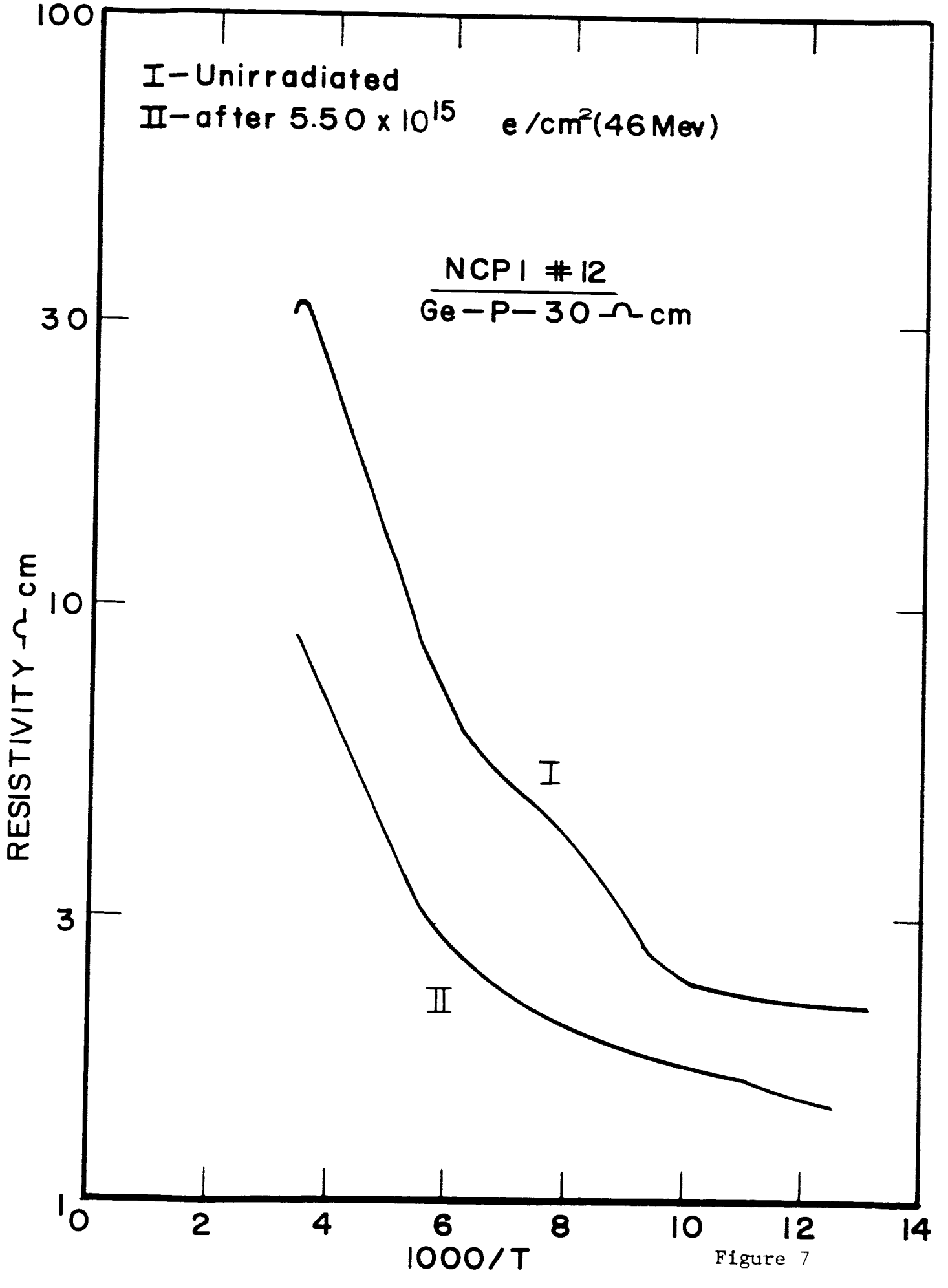
I-Unirradiated
II-after 5.50 x 10^15 e/cm^2(46 Mev)
NCP1 #12
Ge-P-30 Ω cm
RESISTIVITY Ω cm
100
30
10
3
1
0
2
4
6
8
10
12
14
1000/T
I
II

Figure 7

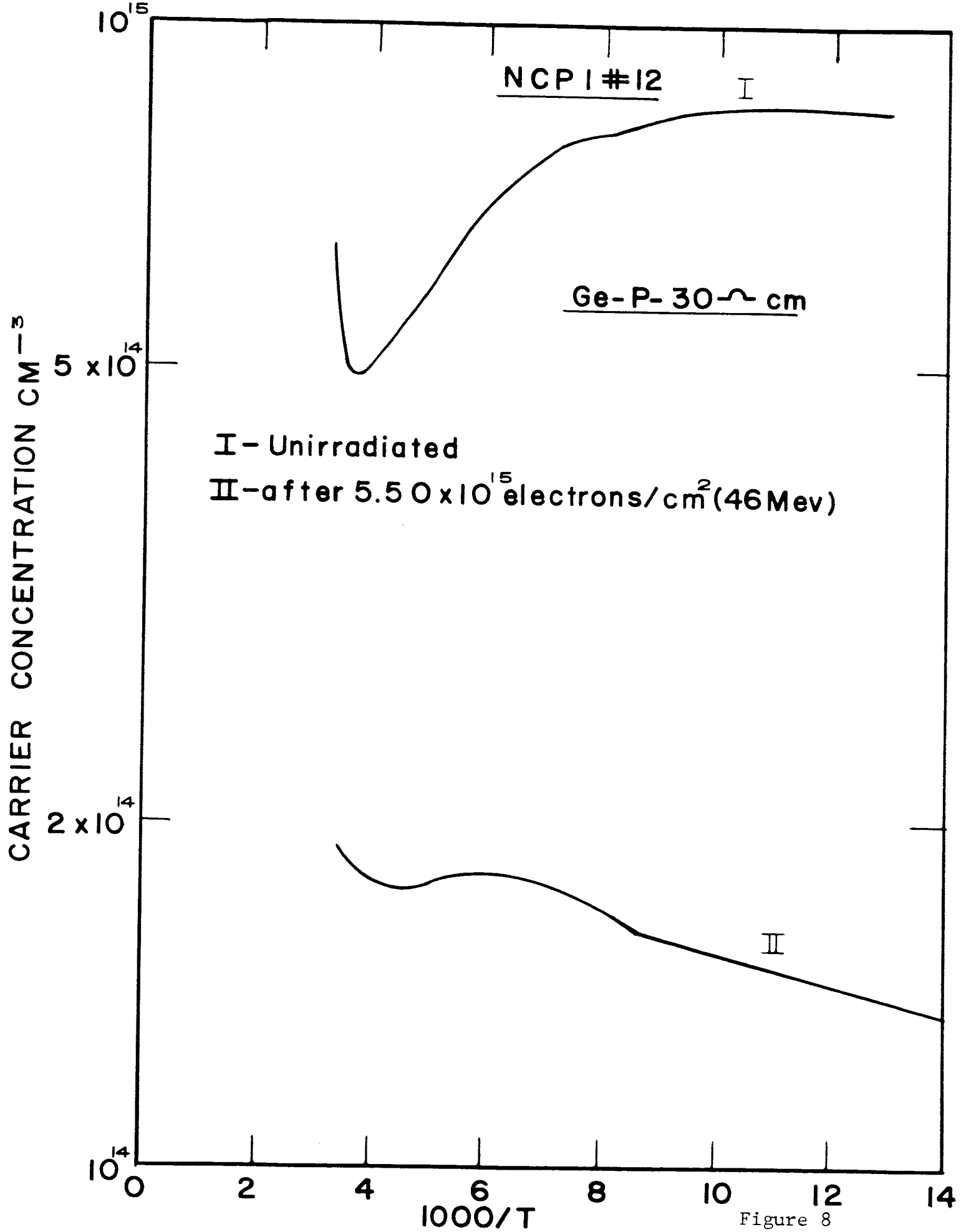
NCP 1 #12
I
Ge-P-30 Ω cm
I- Unirradiated
II-after 5.50 x 10^15 electrons/cm^2 (46 Mev)
II
CARRIER CONCENTRATION CM^-3
10^15
5 x 10^14
2 x 10^14
10^14
0
2
4
6
8
10
12
14
1000/T

Figure 8

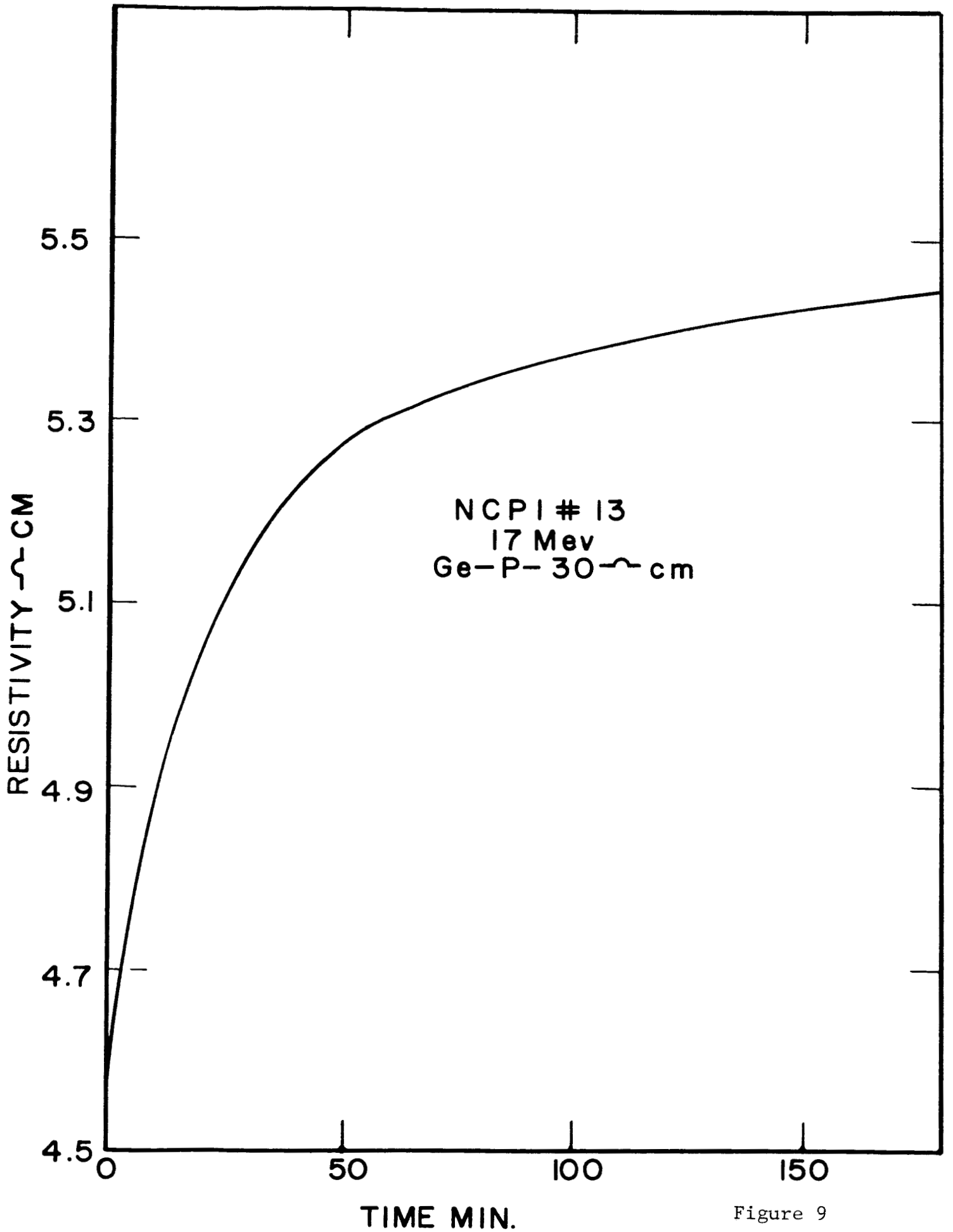
5.5
5.3
5.1
4.9
4.7
4.5
RESISTIVITY ~ CM
NCP1 # 13
17 Mev
Ge–P–30 ~ cm
0
50
100
150
TIME MIN.

Figure 9

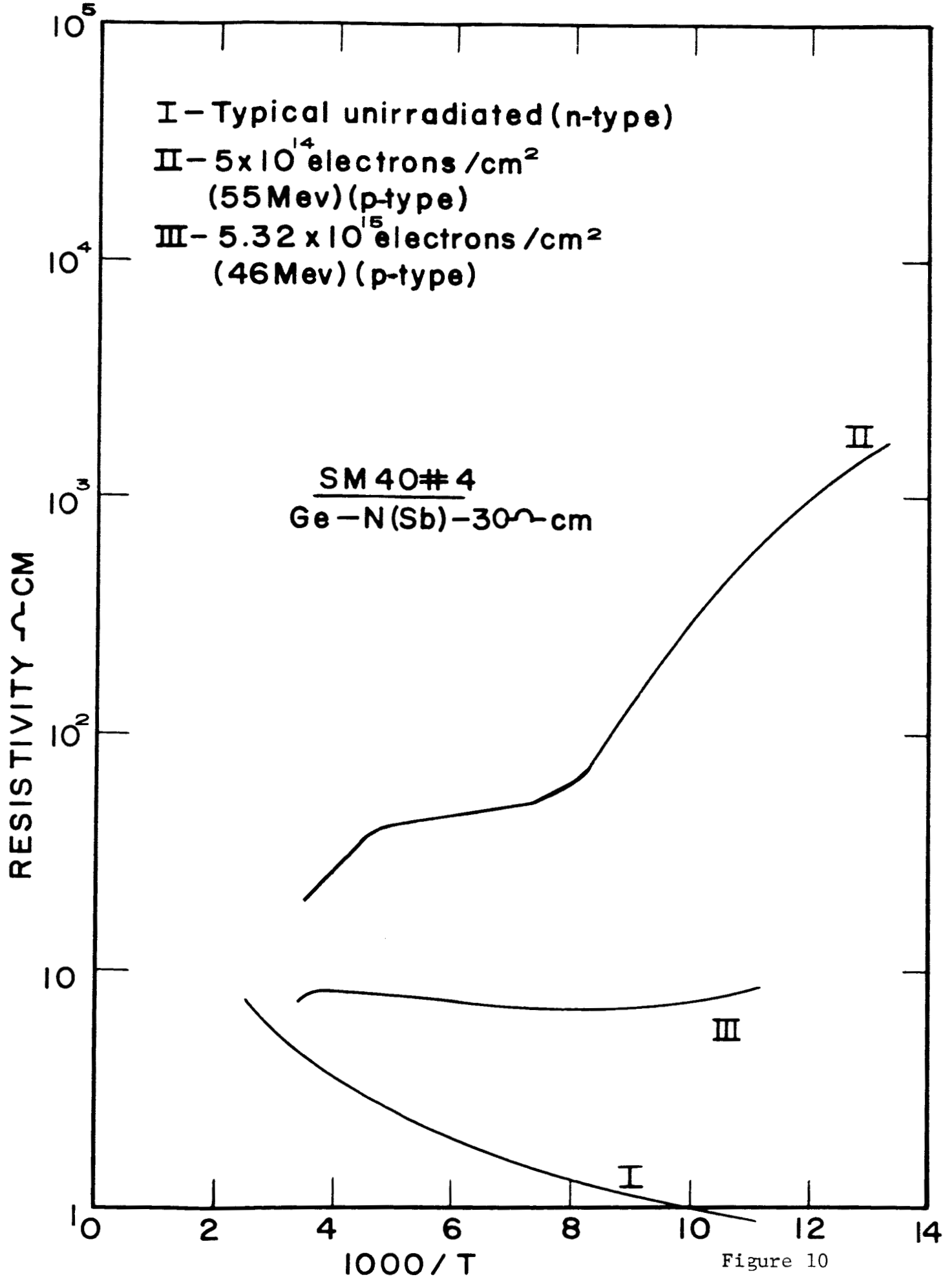
I – Typical unirradiated (n-type)
II – 5x10^14 electrons/cm^2 (55 Mev) (p-type)
III – 5.32 x 10^15 electrons/cm^2 (46 Mev) (p-type)
SM 40 # 4
Ge – N(Sb) – 30Ω-cm
RESISTIVITY Ω-CM
1000/T
I
II
III

Figure 10

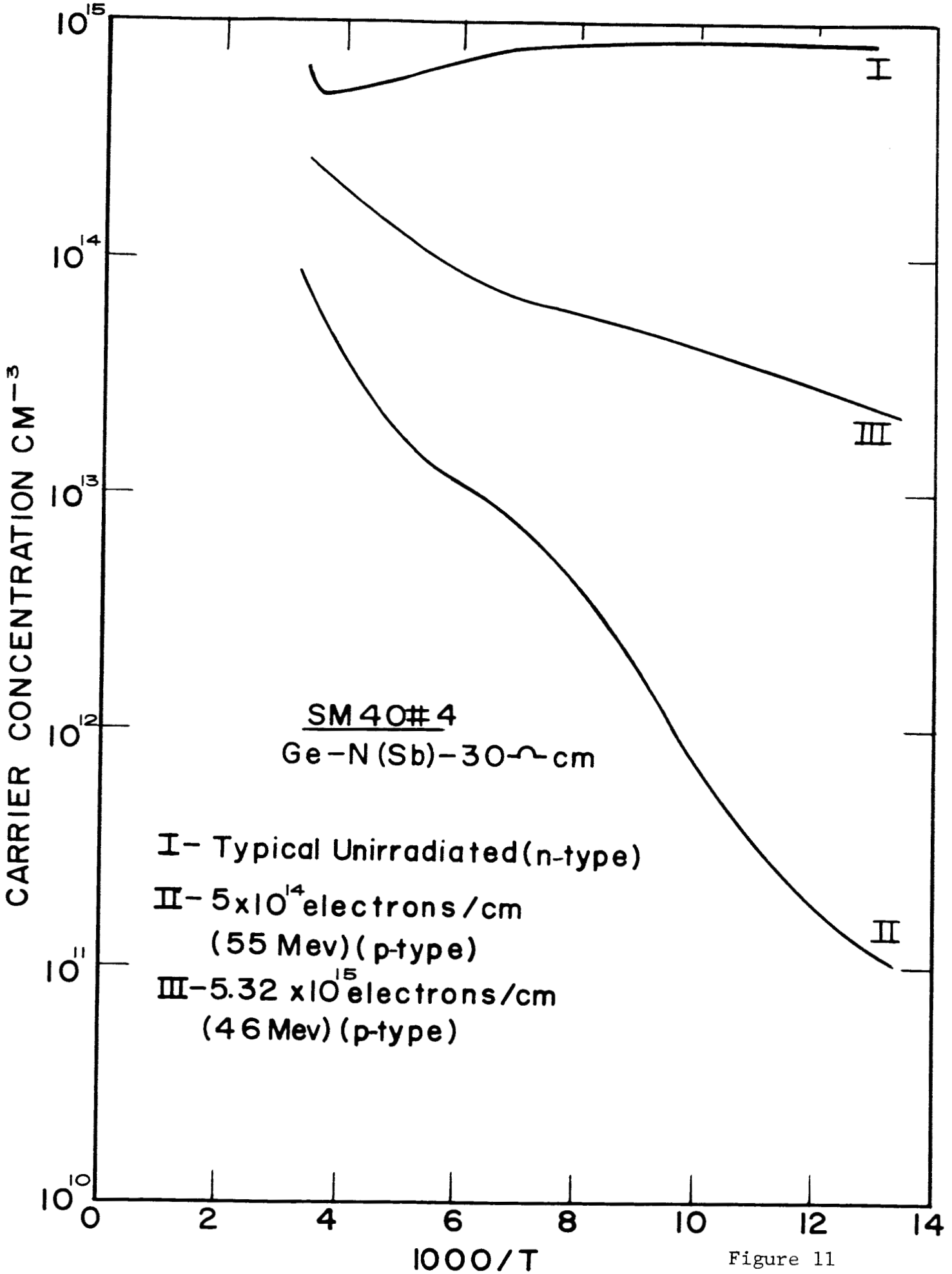
CARRIER CONCENTRATION CM⁻³
10¹⁵
10¹⁴
10¹³
10¹²
10¹¹
10¹⁰
0
2
4
6
8
10
12
14
1000/T
I
II
III
SM 40#4
Ge-N (Sb)-30-Ω-cm
I- Typical Unirradiated (n-type)
II- 5x10¹⁴ electrons/cm (55 Mev) (p-type)
III- 5.32 x10¹⁵ electrons/cm (46 Mev) (p-type)

Figure 11

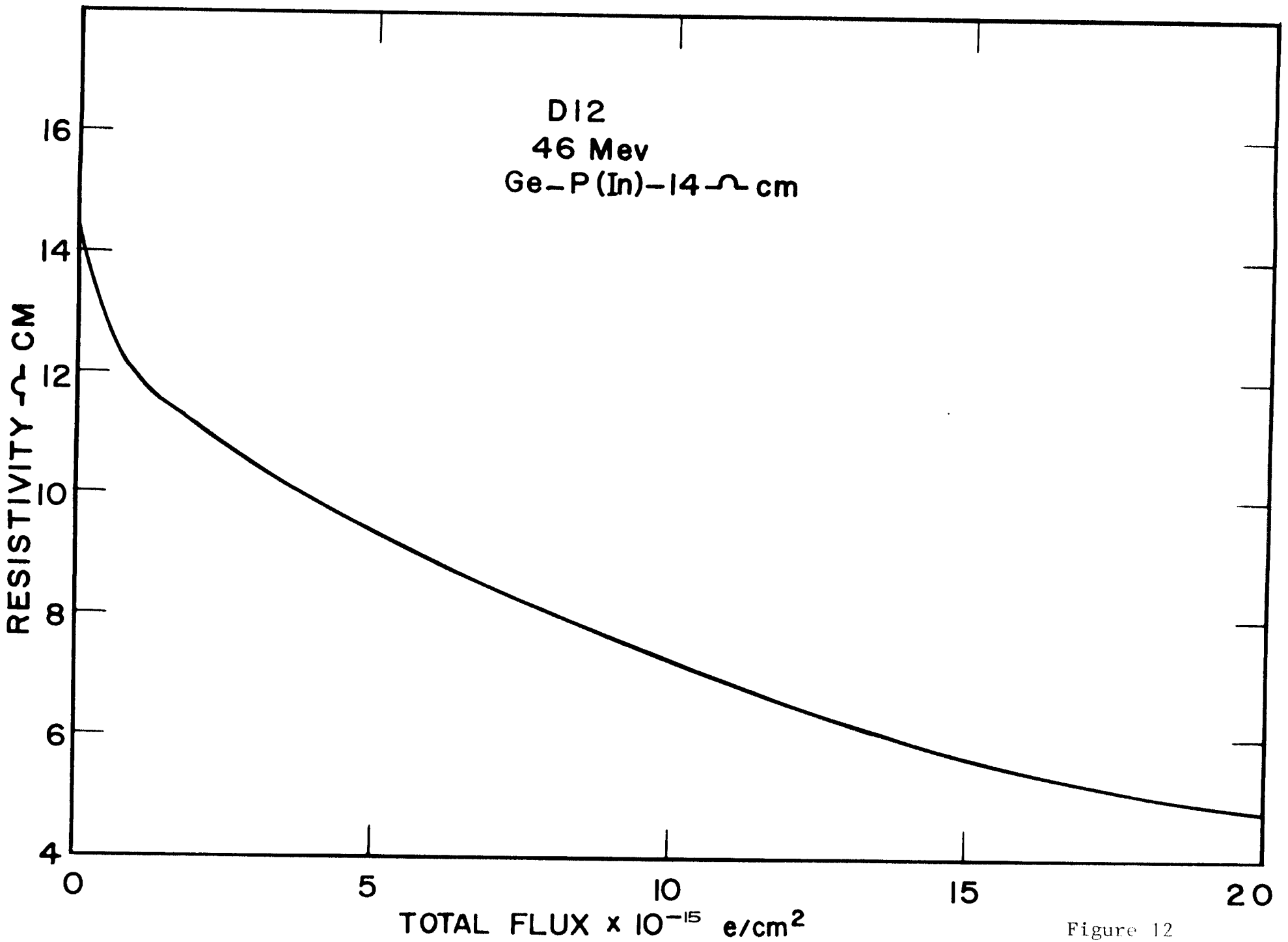
D12
46 Mev
Ge–P(In)–14 Ω cm
RESISTIVITY Ω CM
16
14
12
10
8
6
4
0
5
10
15
20
TOTAL FLUX x 10⁻¹⁵ e/cm²

Figure 12

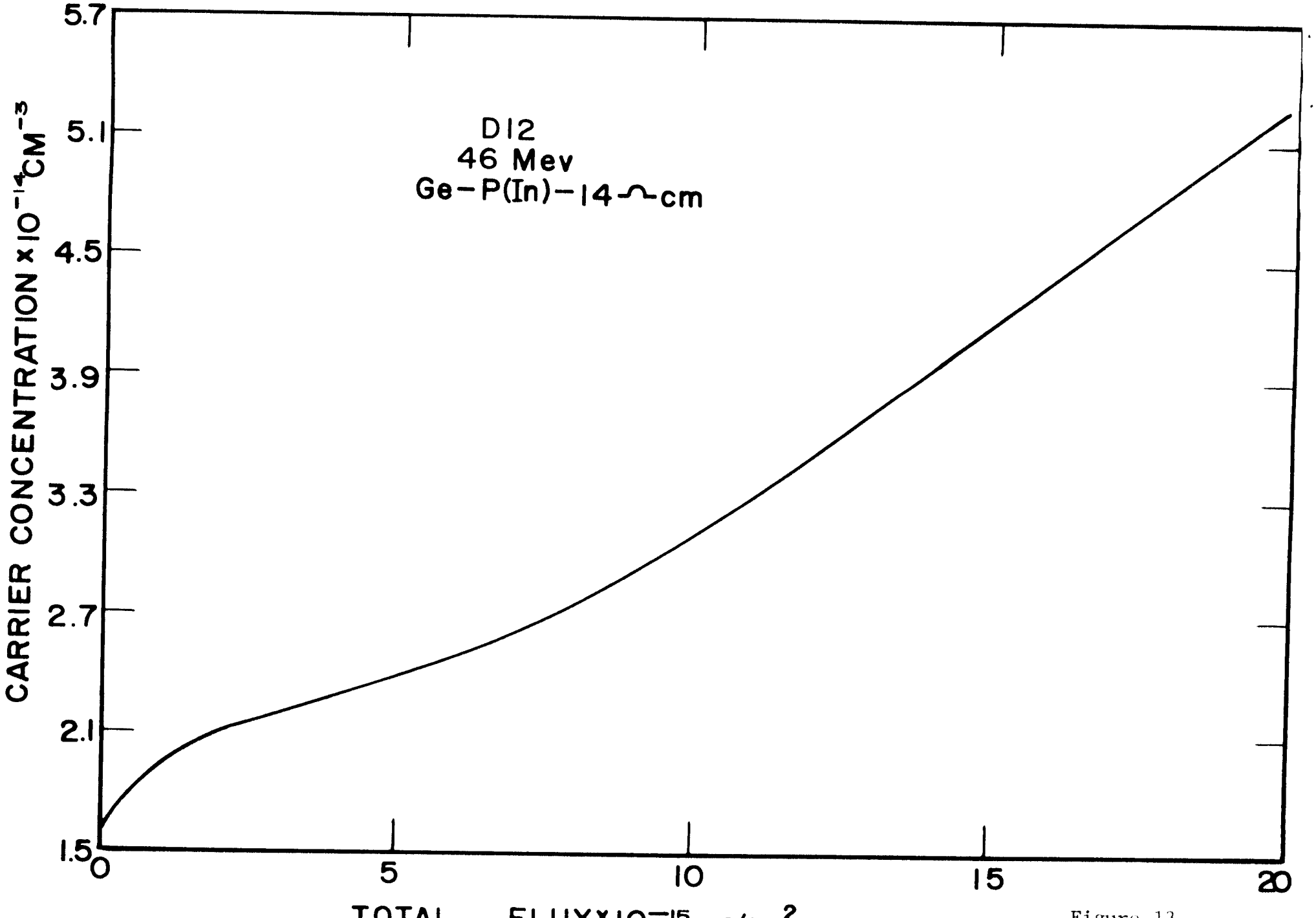
D12
46 Mev
Ge-P(In)-14-Ω-cm
CARRIER CONCENTRATION x10⁻¹⁴CM⁻³
5.7
5.1
4.5
3.9
3.3
2.7
2.1
1.5
0
5
10
15
20
TOTAL FLUX x10⁻¹⁵ e/cm²

Figure 13

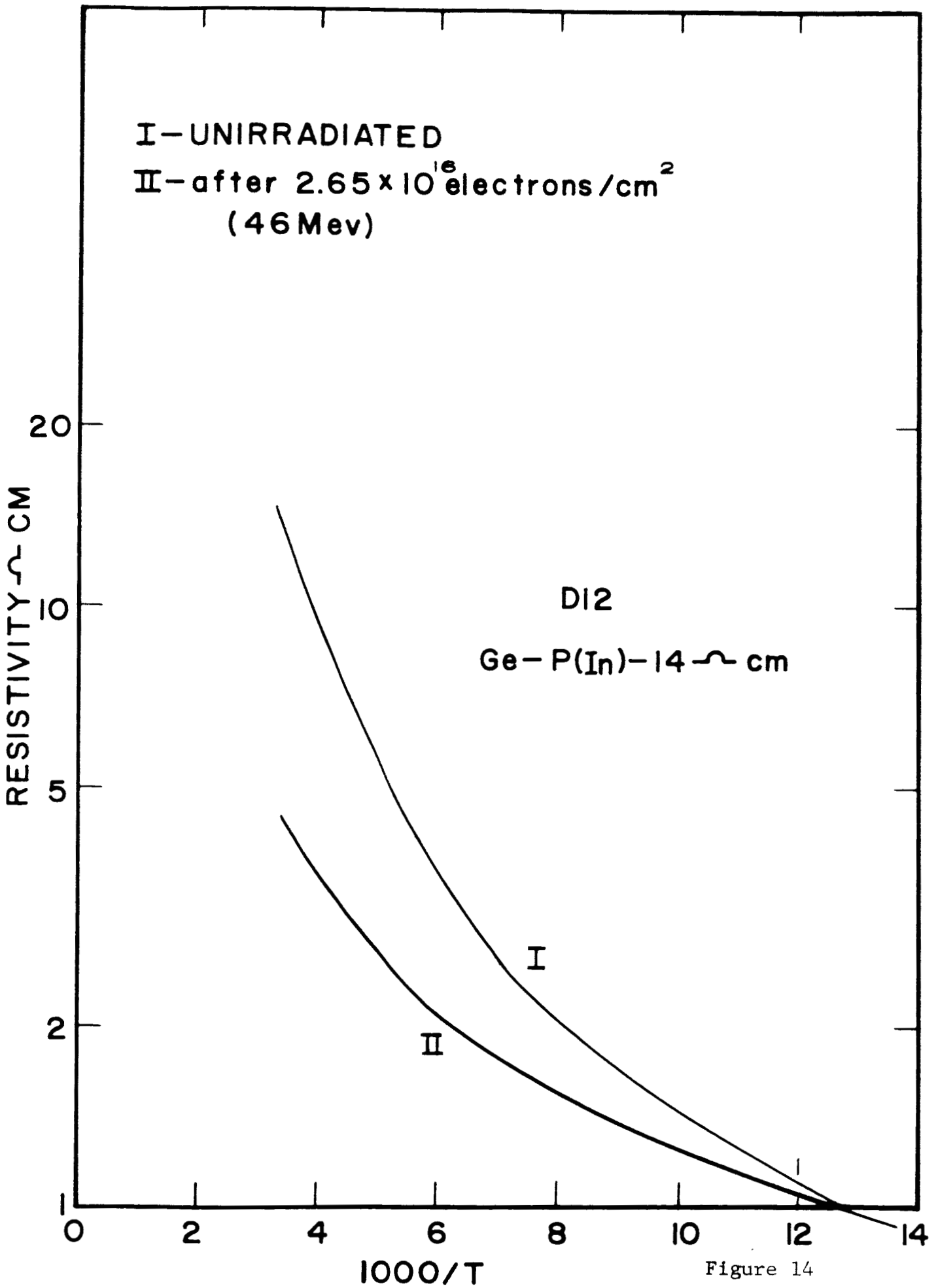
I-UNIRRADIATED
II-after 2.65 x 10^16 electrons/cm^2
(46 Mev)
D12
Ge-P(In)-14 Ω cm
RESISTIVITY-Ω CM
20
10
5
2
1
0
2
4
6
8
10
12
14
1000/T
I
II

Figure 14

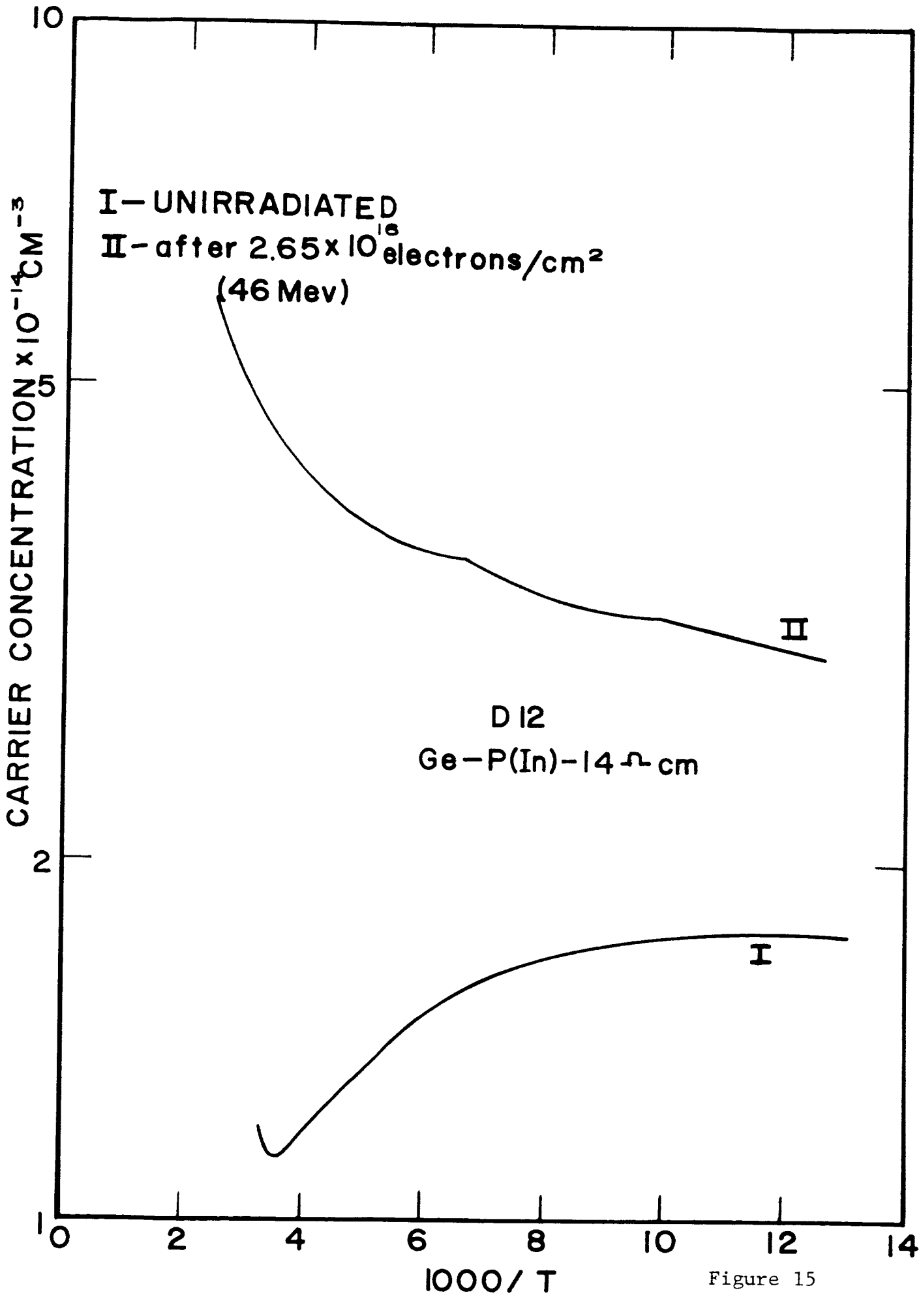
I – UNIRRADIATED
II – after 2.65 x 10^16 electrons/cm²
(46 Mev)
D 12
Ge – P(In) – 14 Ω-cm
CARRIER CONCENTRATION x 10^-14 CM^-3
1000 / T
10
5
2
1
0
2
4
6
8
10
12
14
I
II

Figure 15

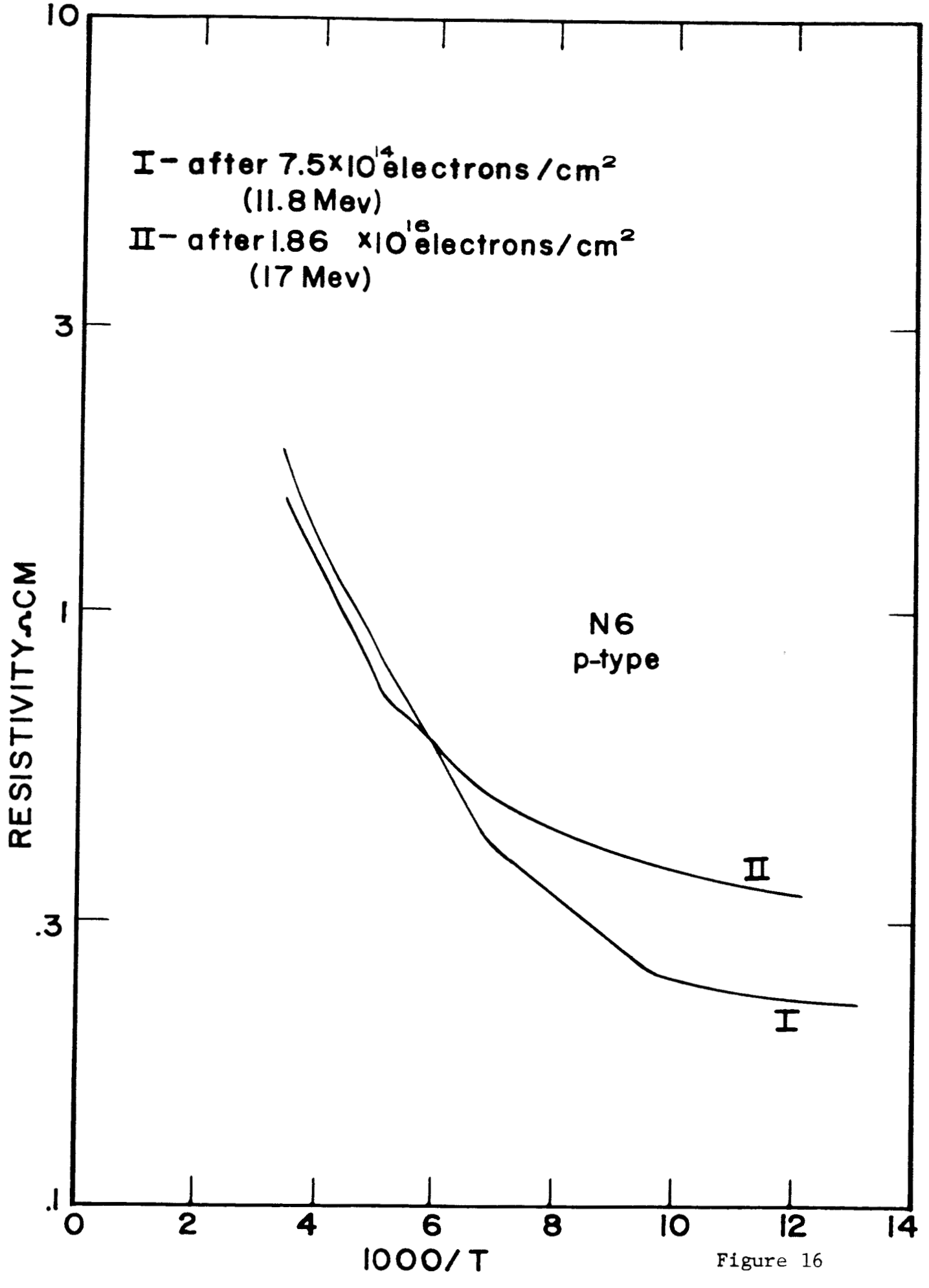
I- after 7.5x10^14 electrons/cm^2
(11.8 Mev)
II- after 1.86 x10^16 electrons/cm^2
(17 Mev)
N6
p-type
II
I
RESISTIVITY-Ω CM
10
3
1
.3
.1
0
2
4
6
8
10
12
14
1000/T

Figure 16

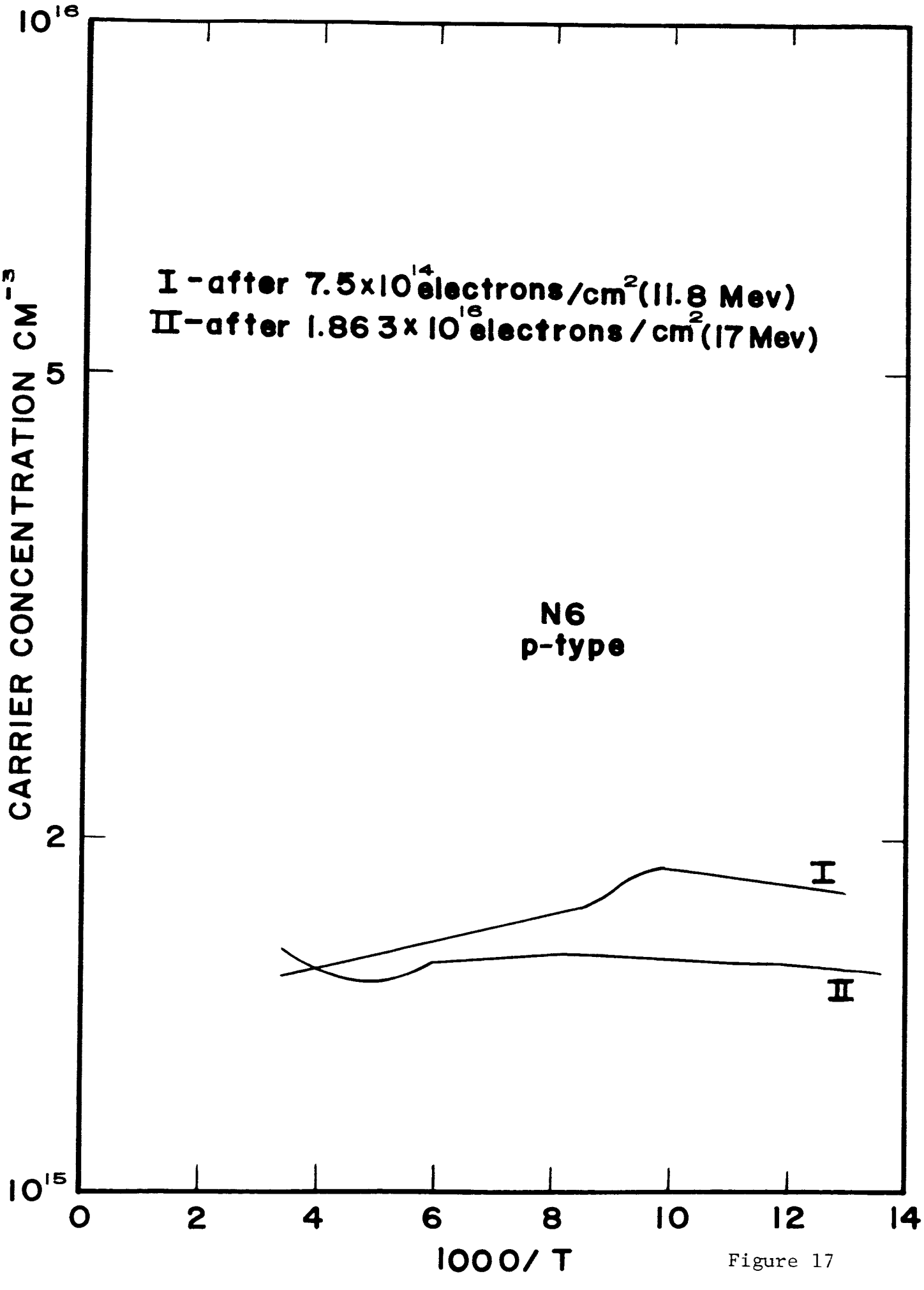
I - after 7.5x10^14 electrons/cm^2 (11.8 Mev)
II - after 1.863x10^16 electrons/cm^2 (17 Mev)
N6
p-type
CARRIER CONCENTRATION CM^-3
10^16
5
2
10^15
I
II
0
2
4
6
8
10
12
14
1000/T

Figure 17

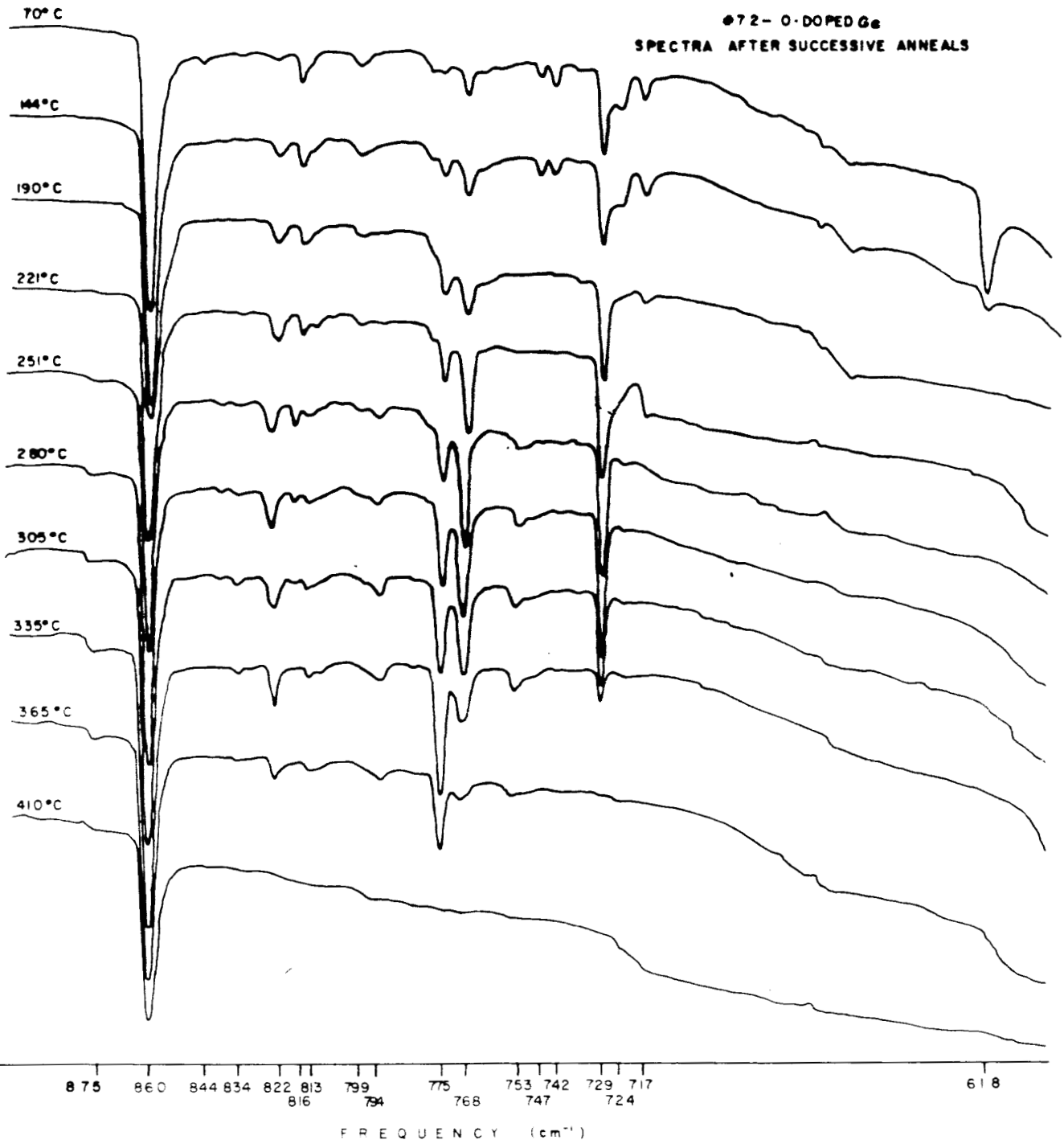
70° C
144°C
190°C
221°C
251°C
280°C
305°C
335°C
365°C
410°C
#72 - O-DOPED Ge
SPECTRA AFTER SUCCESSIVE ANNEALS
875
860
844
834
822
816
813
799
794
775
768
753
747
742
729
724
717
618
FREQUENCY (cm⁻¹)

Figure 18

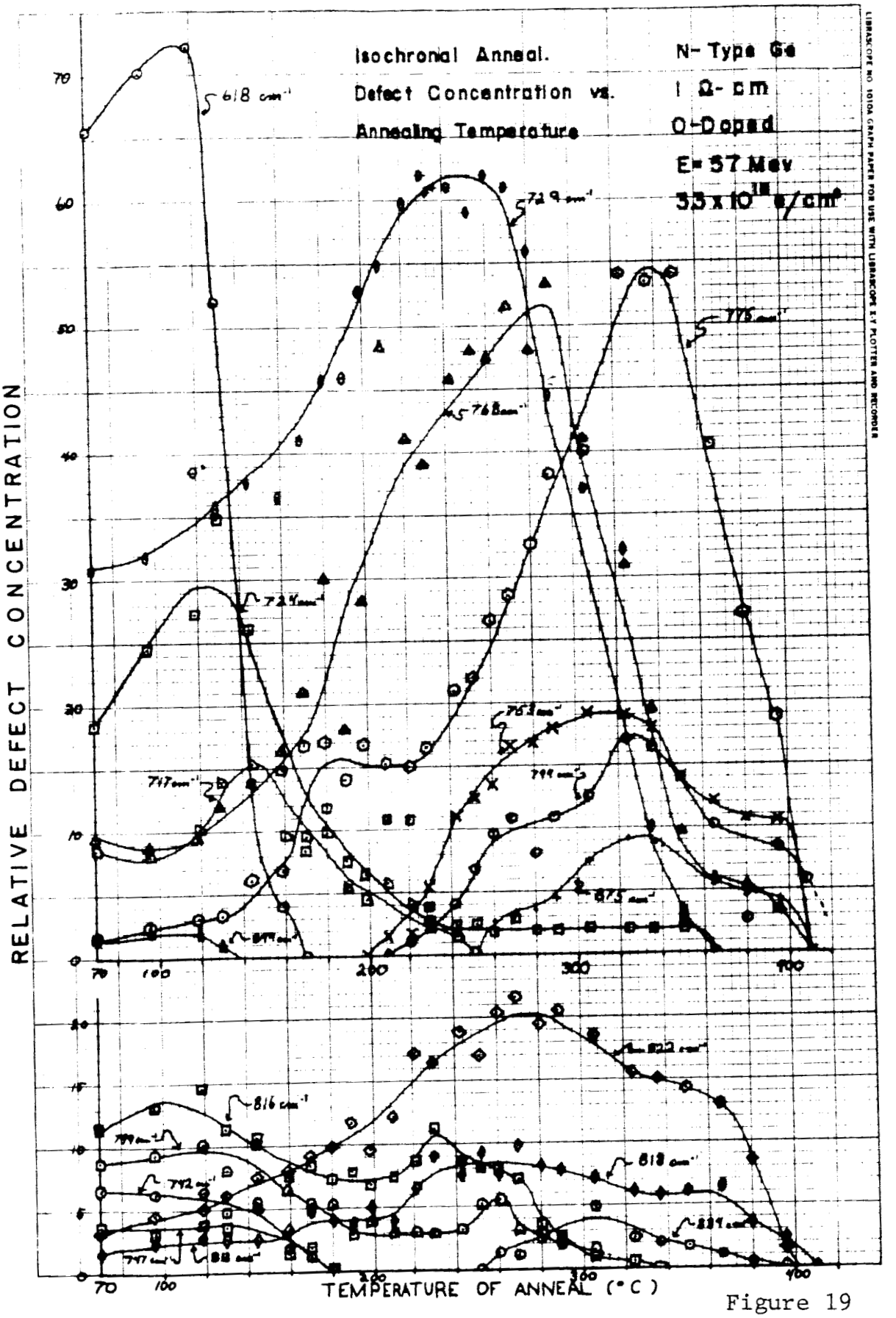
Isochronal Anneal.
Defect Concentration vs.
Annealing Temperature
N-Type Ge
1 Ω-cm
O-Doped
E= 57 Mev
3.3x10^18 e/cm^2
618 cm^-1
729 cm^-1
775 cm^-1
768 cm^-1
734 cm^-1
753 cm^-1
717 cm^-1
799 cm^-1
875 cm^-1
877 cm^-1
816 cm^-1
822 cm^-1
818 cm^-1
799 cm^-1
792 cm^-1
747 cm^-1
RELATIVE DEFECT CONCENTRATION
TEMPERATURE OF ANNEAL (°C)
70
100
200
300
400

Figure 19

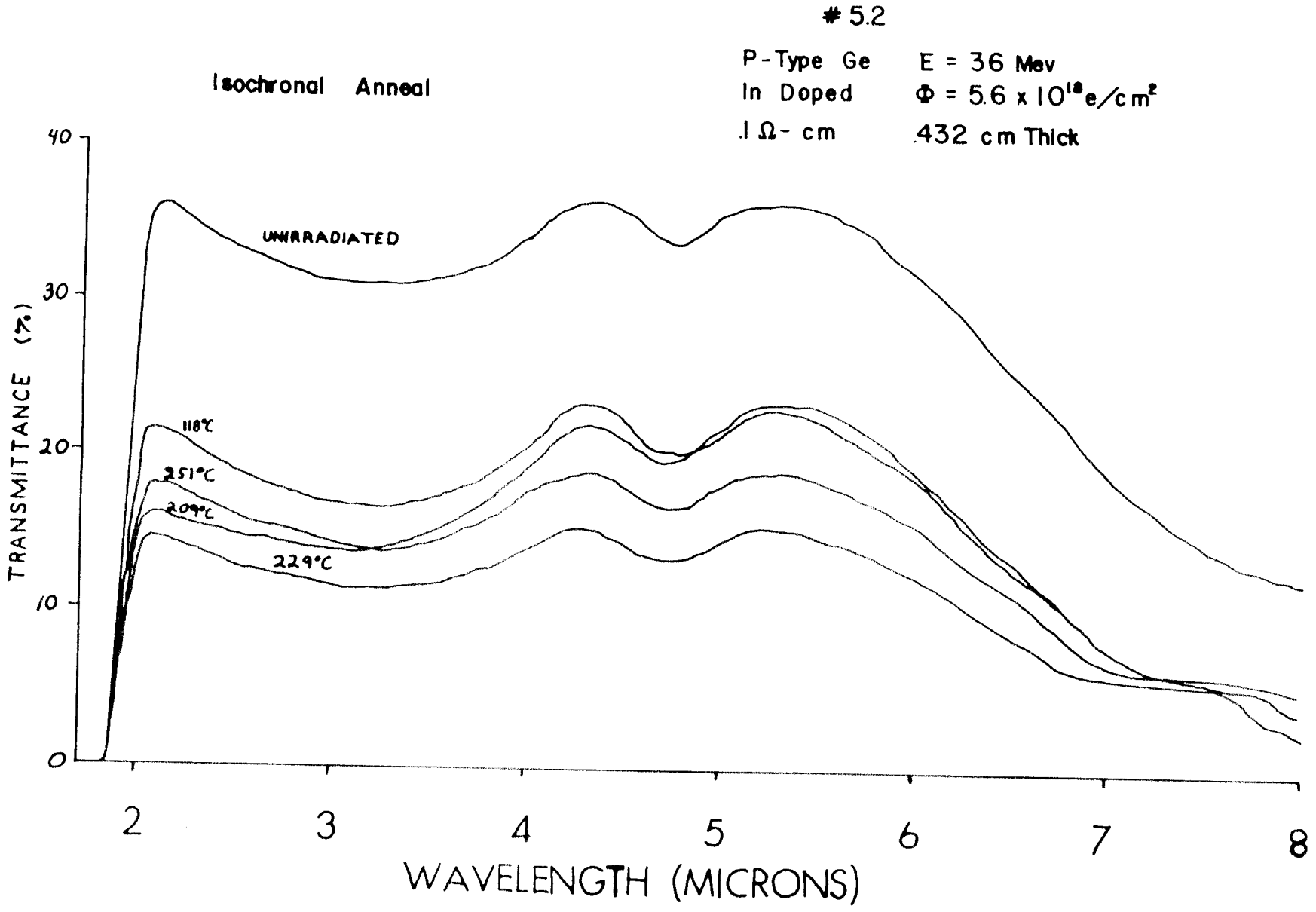
#5.2
P-Type Ge
In Doped
.1 Ω- cm
E = 36 Mev
Φ = 5.6 x 10^18 e/cm^2
.432 cm Thick
Isochronal Anneal
UNIRRADIATED
118°C
251°C
209°C
229°C
TRANSMITTANCE (%)
40
30
20
10
0
2
3
4
5
6
7
8
WAVELENGTH (MICRONS)

Figure 20

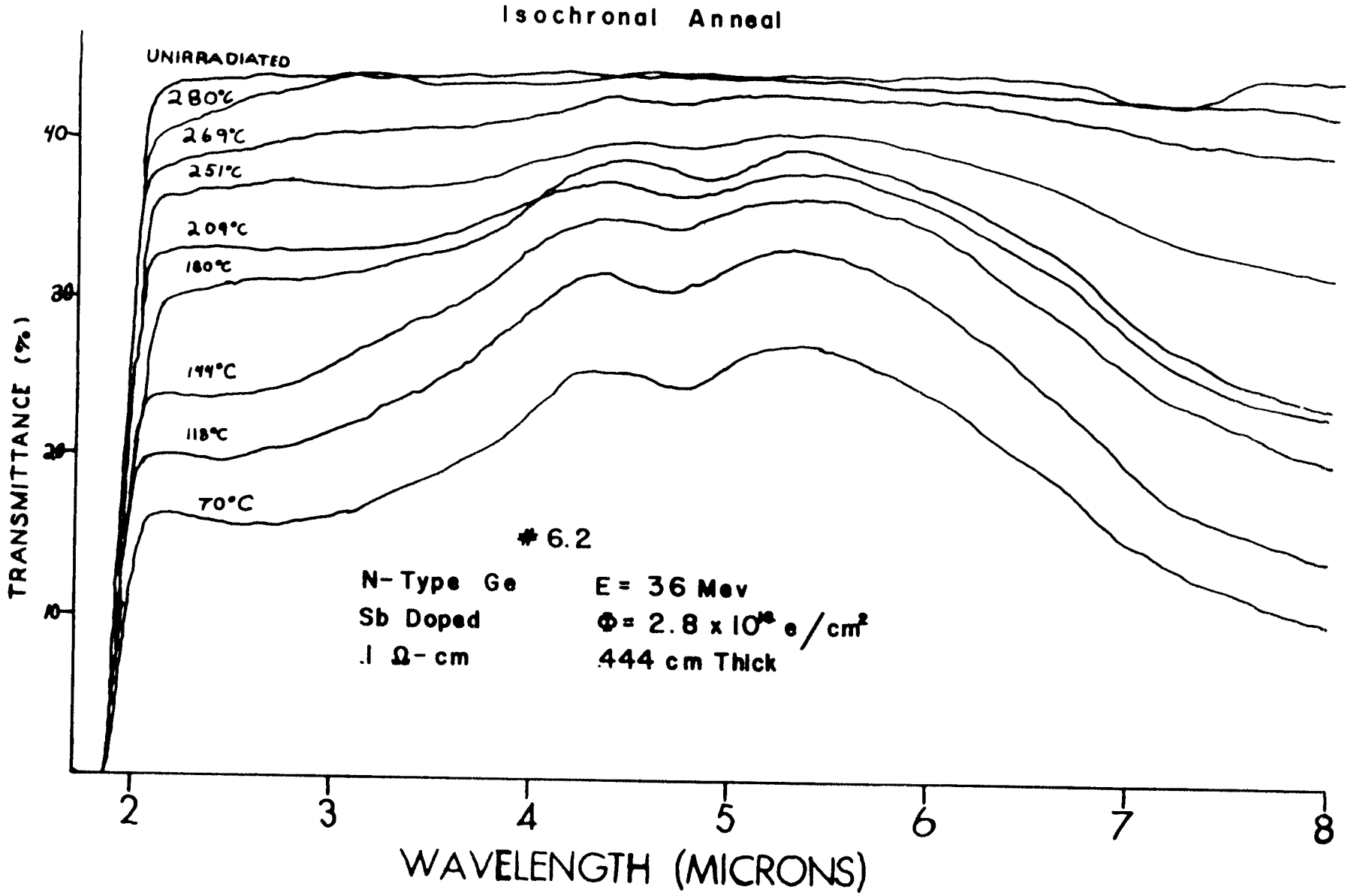
Isochronal Anneal
UNIRRADIATED
280°C
269°C
251°C
209°C
180°C
144°C
118°C
70°C
#6.2
N-Type Ge
Sb Doped
.1 Ω-cm
E = 36 Mev
Φ = 2.8 x 10^16 e/cm^2
444 cm Thick
TRANSMITTANCE (%)
40
30
20
10
2
3
4
5
6
7
8
WAVELENGTH (MICRONS)

Figure 21

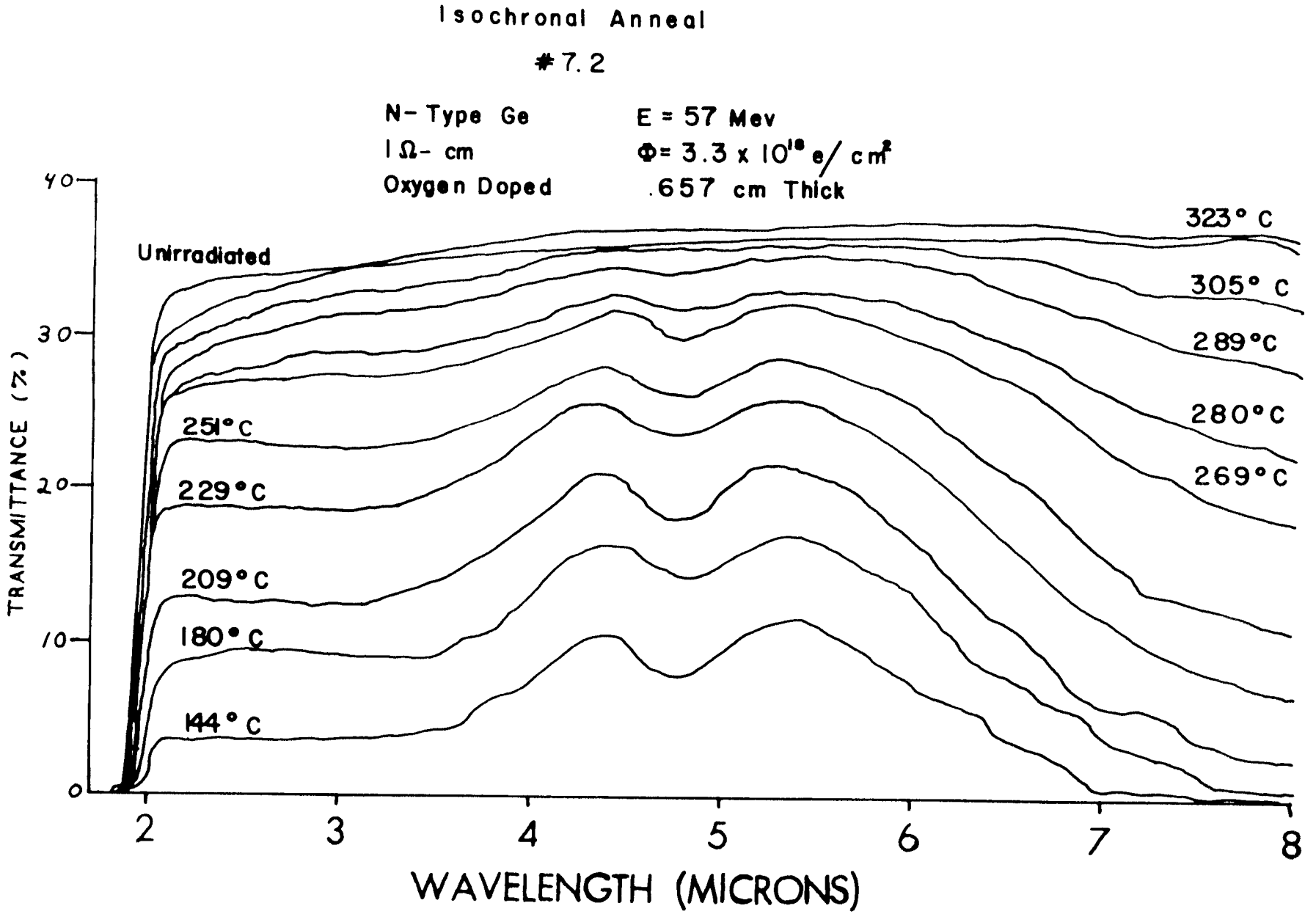
Isochronal Anneal
#7.2
N-Type Ge
1 Ω-cm
Oxygen Doped
E = 57 Mev
Φ = 3.3 x 10^16 e/cm^2
.657 cm Thick
Unirradiated
323° C
305° C
289°C
280°C
269°C
251°C
229°C
209°C
180°C
144°C
TRANSMITTANCE (%)
40
30
20
10
0
2
3
4
5
6
7
8
WAVELENGTH (MICRONS)

Figure 22

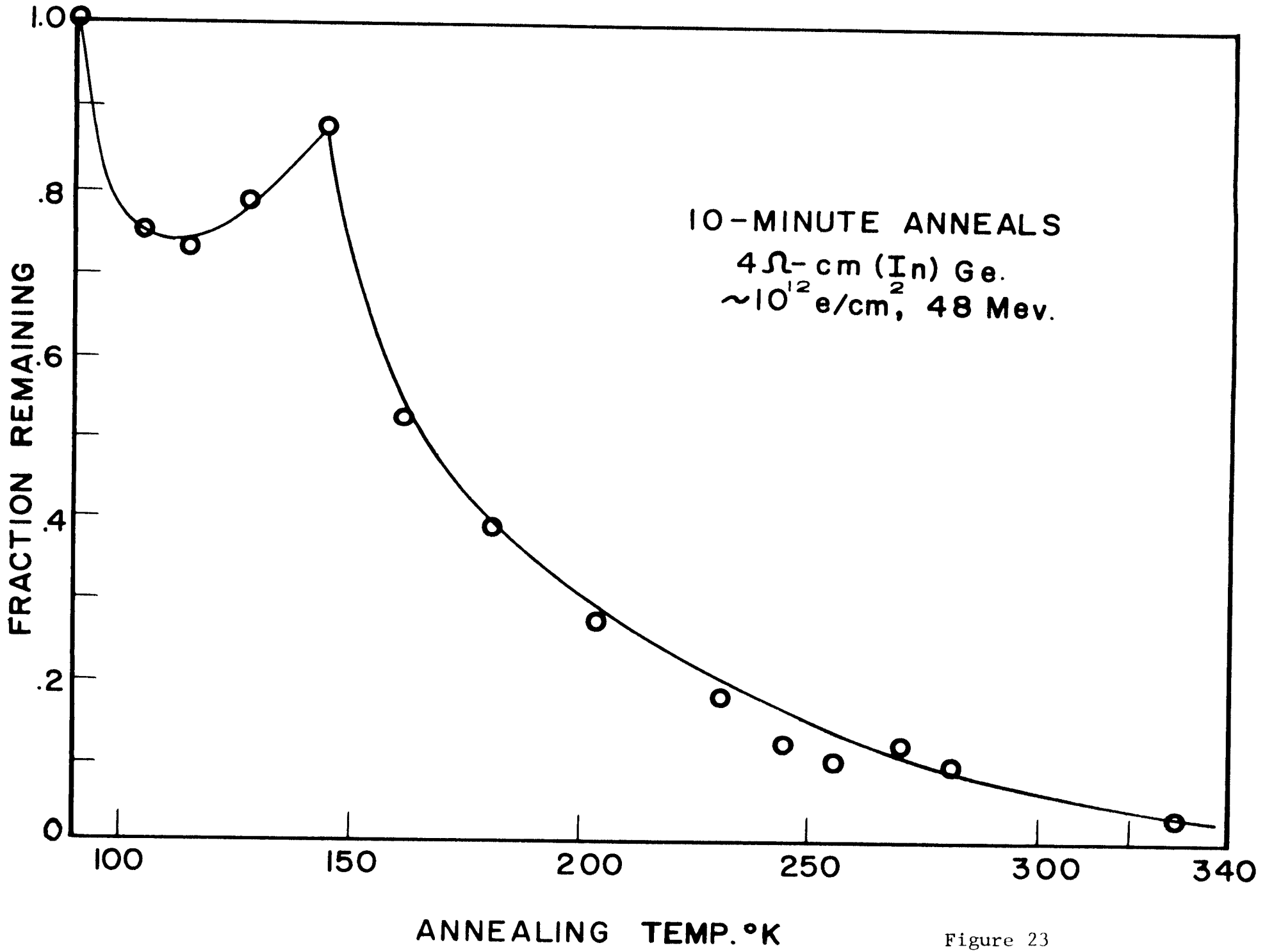
1.0
.8
.6
.4
.2
0
FRACTION REMAINING
10-MINUTE ANNEALS
4Ω-cm (In) Ge.
~10^12 e/cm^2, 48 Mev.
100
150
200
250
300
340
ANNEALING TEMP. °K

Figure 23

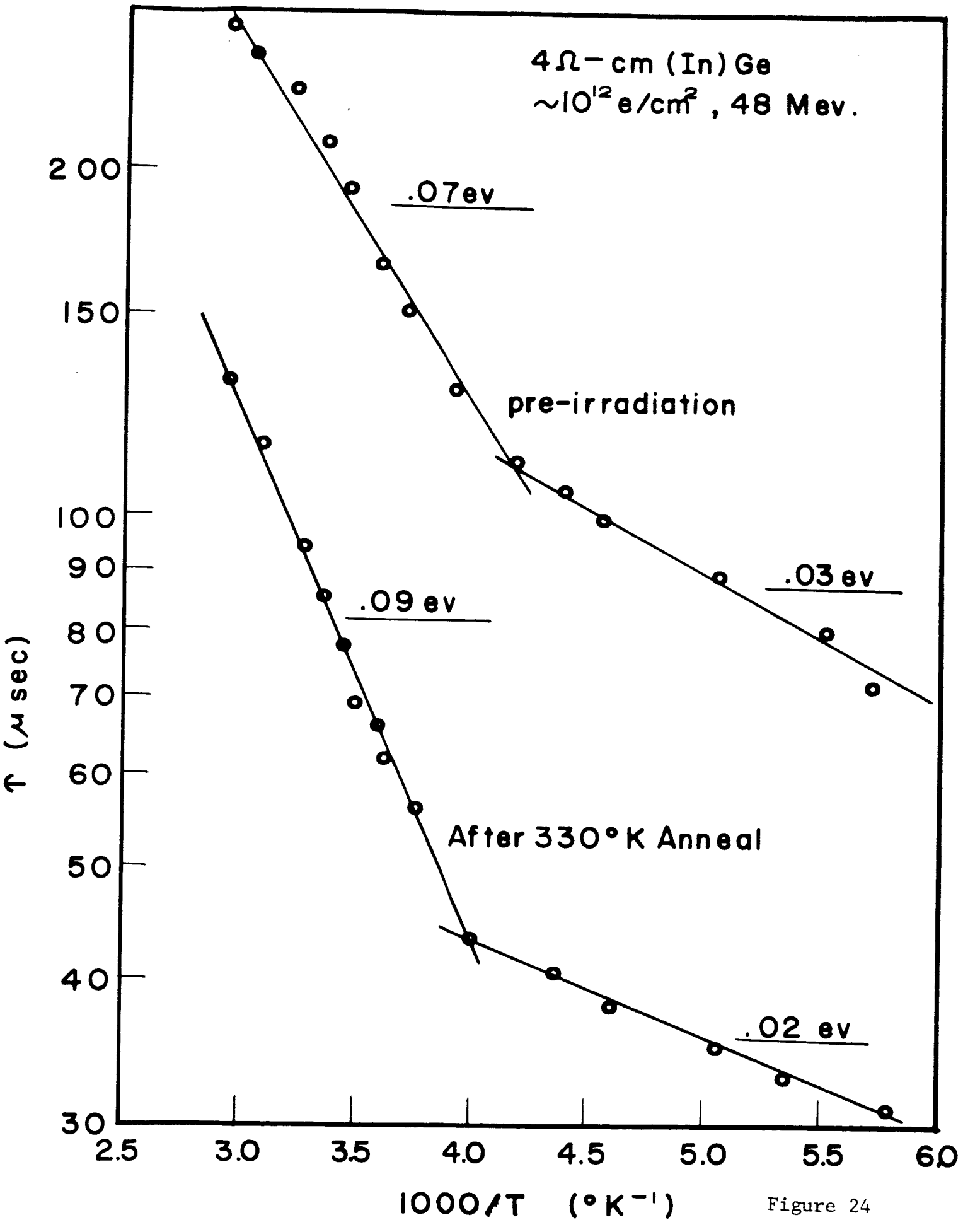
4Ω-cm (In) Ge
~10^12 e/cm^2 , 48 Mev.
.07ev
pre-irradiation
.03 ev
.09 ev
After 330°K Anneal
.02 ev
200
150
100
90
80
70
60
50
40
30
τ (μsec)
2.5
3.0
3.5
4.0
4.5
5.0
5.5
6.0
1000/T (°K^-1)

Figure 24

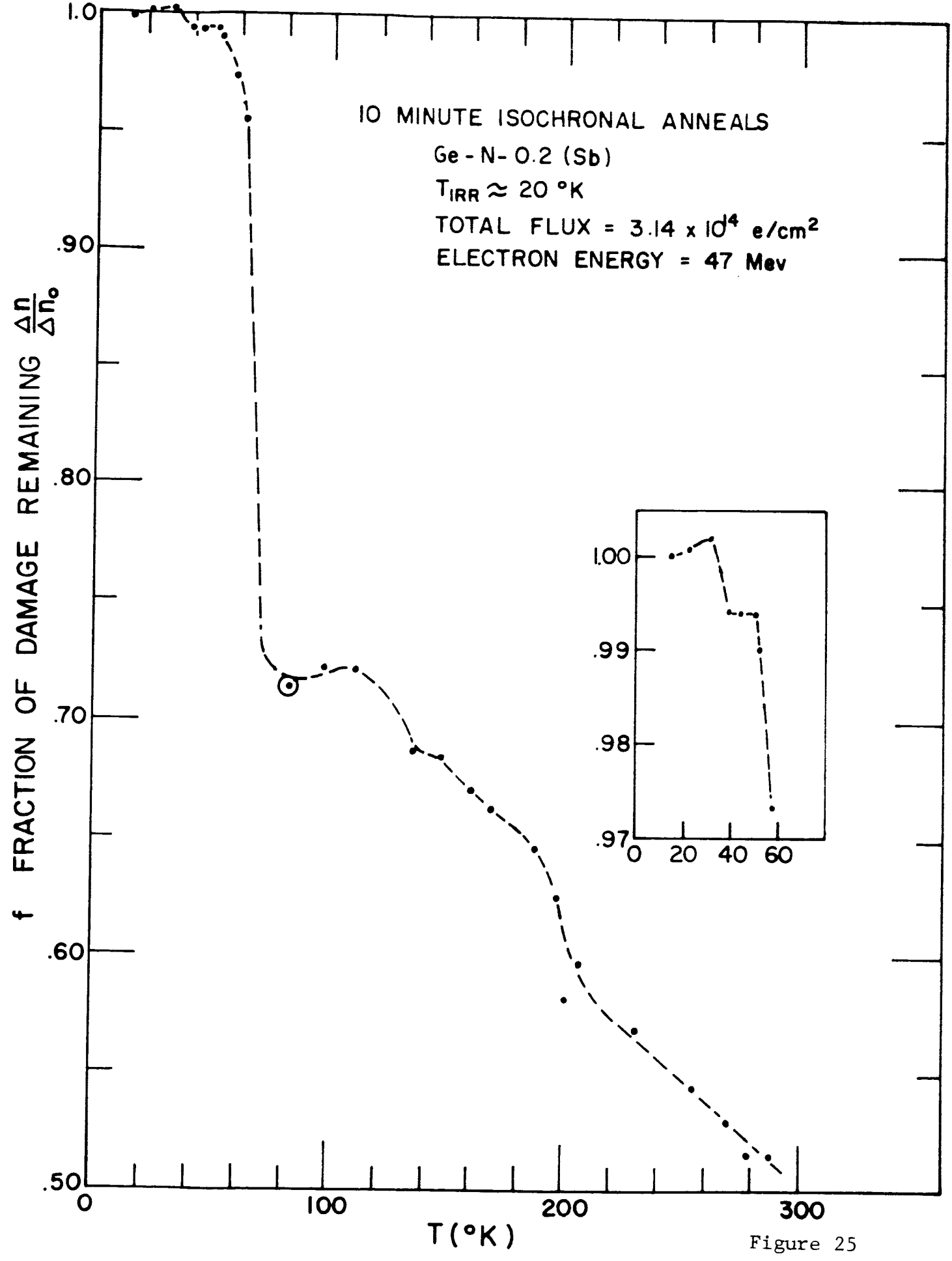
10 MINUTE ISOCHRONAL ANNEALS
Ge - N - 0.2 (Sb)
$T_{IRR} \approx 20$ °K
TOTAL FLUX = 3.14×10^{14} e/cm²
ELECTRON ENERGY = 47 Mev
f FRACTION OF DAMAGE REMAINING $\frac{\Delta n}{\Delta n_o}$
1.0
.90
.80
.70
.60
.50
0
100
200
300
T(°K)
1.00
.99
.98
.97
0
20
40
60

Figure 25

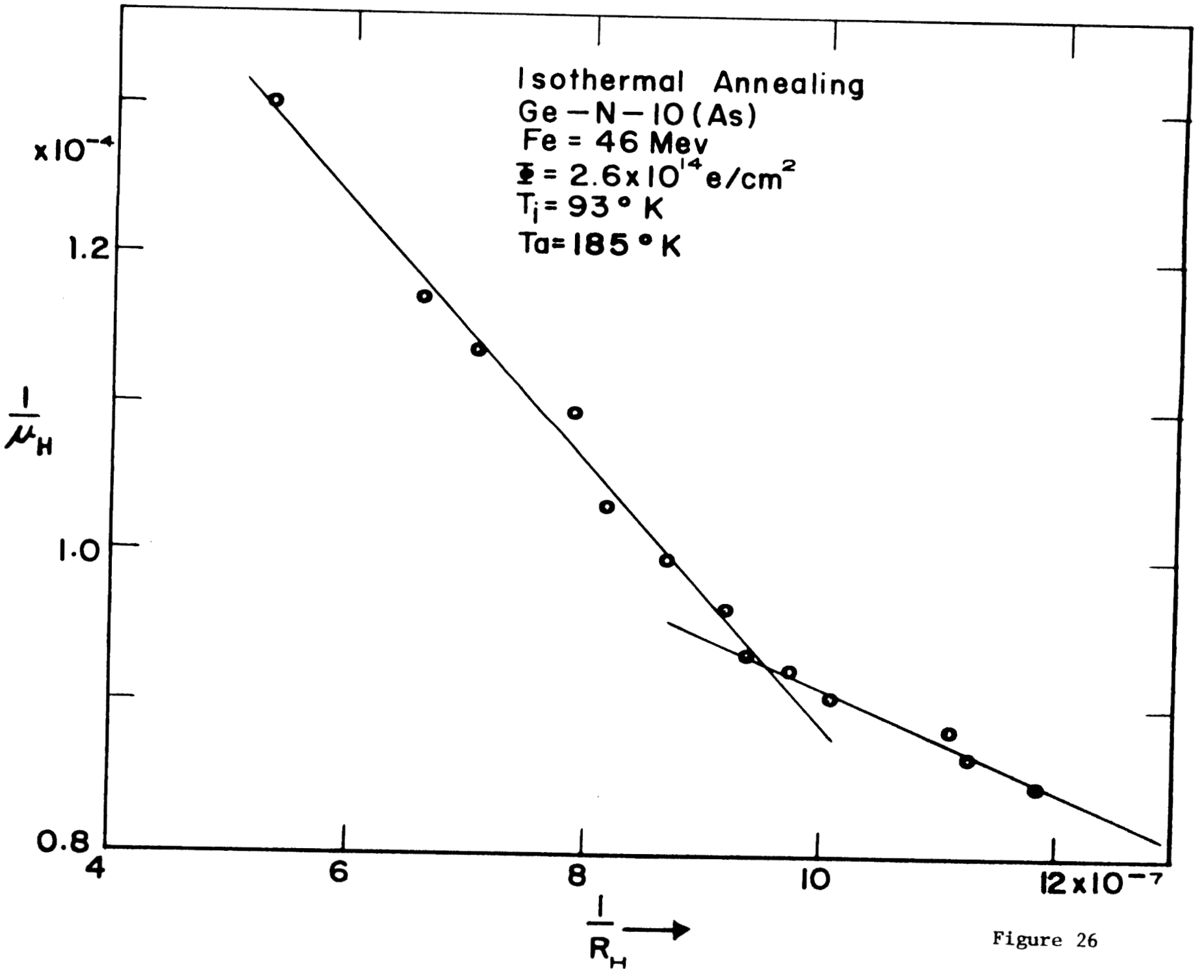
Isothermal Annealing
Ge – N – 10 (As)
Fe = 46 Mev
Φ = 2.6x10^14 e/cm^2
Ti = 93° K
Ta = 185° K
x10^-4
1.2
1.0
0.8
1/μH
4
6
8
10
12x10^-7
1/RH

Figure 26

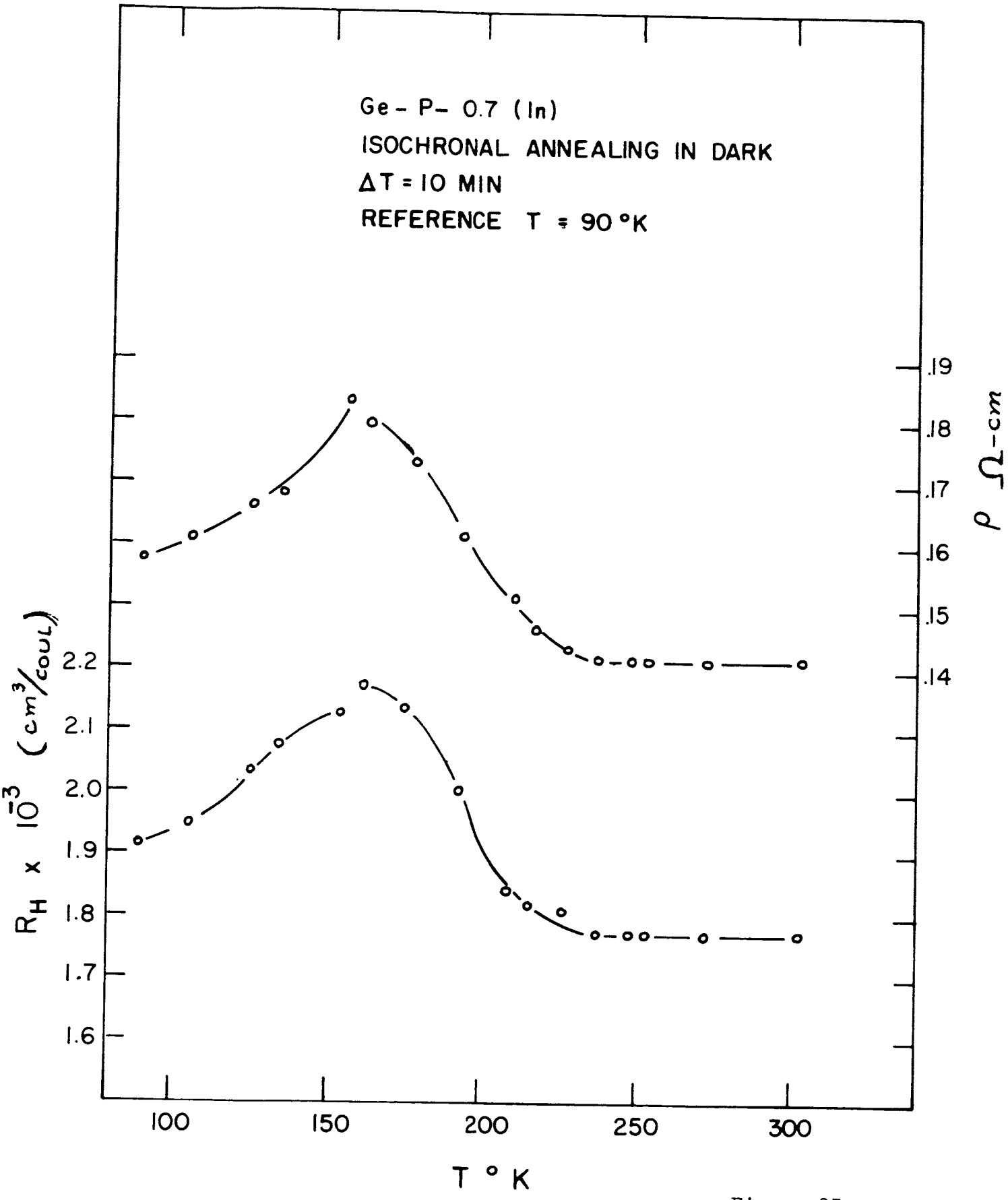
Ge - P - 0.7 (In)
ISOCHRONAL ANNEALING IN DARK
ΔT = 10 MIN
REFERENCE T = 90 °K
$R_H \times 10^{-3}$ (cm^3/coul)
2.2
2.1
2.0
1.9
1.8
1.7
1.6
.19
.18
.17
.16
.15
.14
ρ Ω-cm
100
150
200
250
300
T °K

Figure 27

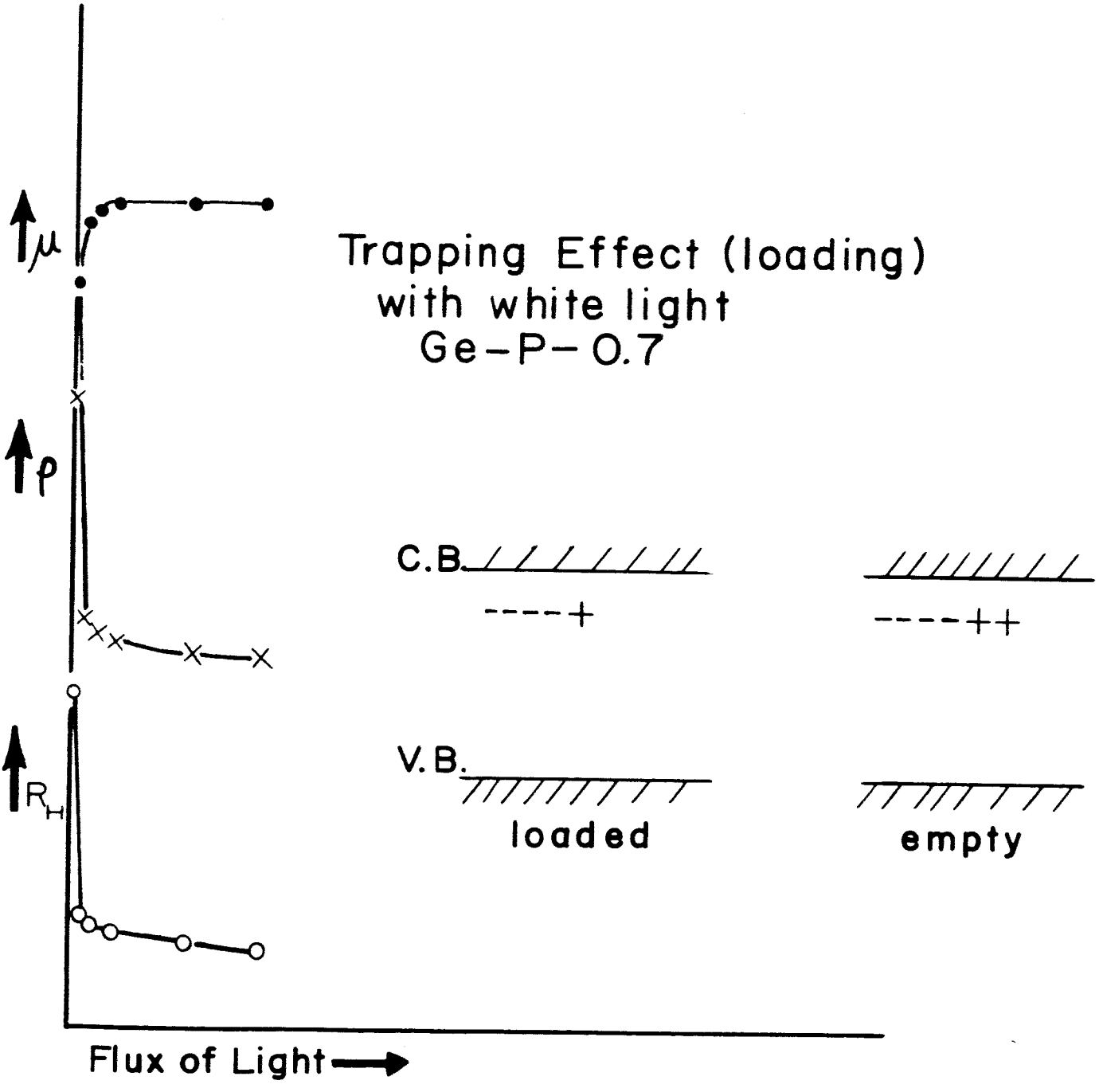
Trapping Effect (loading)
with white light
Ge-P-0.7
μ
ρ
R_H
C.B
----+
----++
V.B.
loaded
empty
Flux of Light

Figure 28

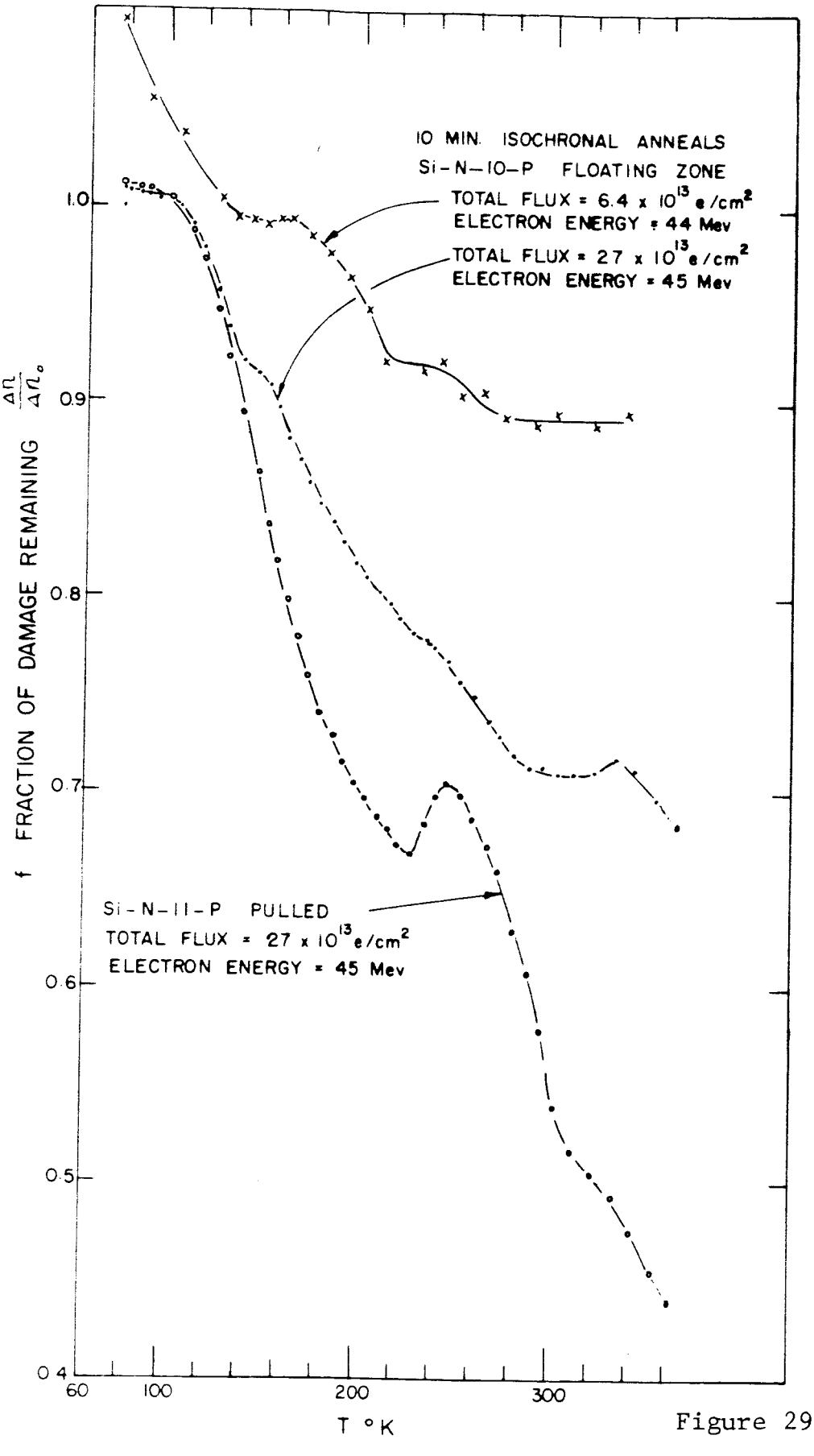
10 MIN. ISOCHRONAL ANNEALS
Si-N-10-P FLOATING ZONE
TOTAL FLUX = 6.4 x 10^13 e/cm^2
ELECTRON ENERGY = 44 Mev
TOTAL FLUX = 27 x 10^13 e/cm^2
ELECTRON ENERGY = 45 Mev
Si-N-11-P PULLED
TOTAL FLUX = 27 x 10^13 e/cm^2
ELECTRON ENERGY = 45 Mev
f FRACTION OF DAMAGE REMAINING Δn/Δn₀
1.0
0.9
0.8
0.7
0.6
0.5
0.4
60
100
200
300
T °K

Figure 29

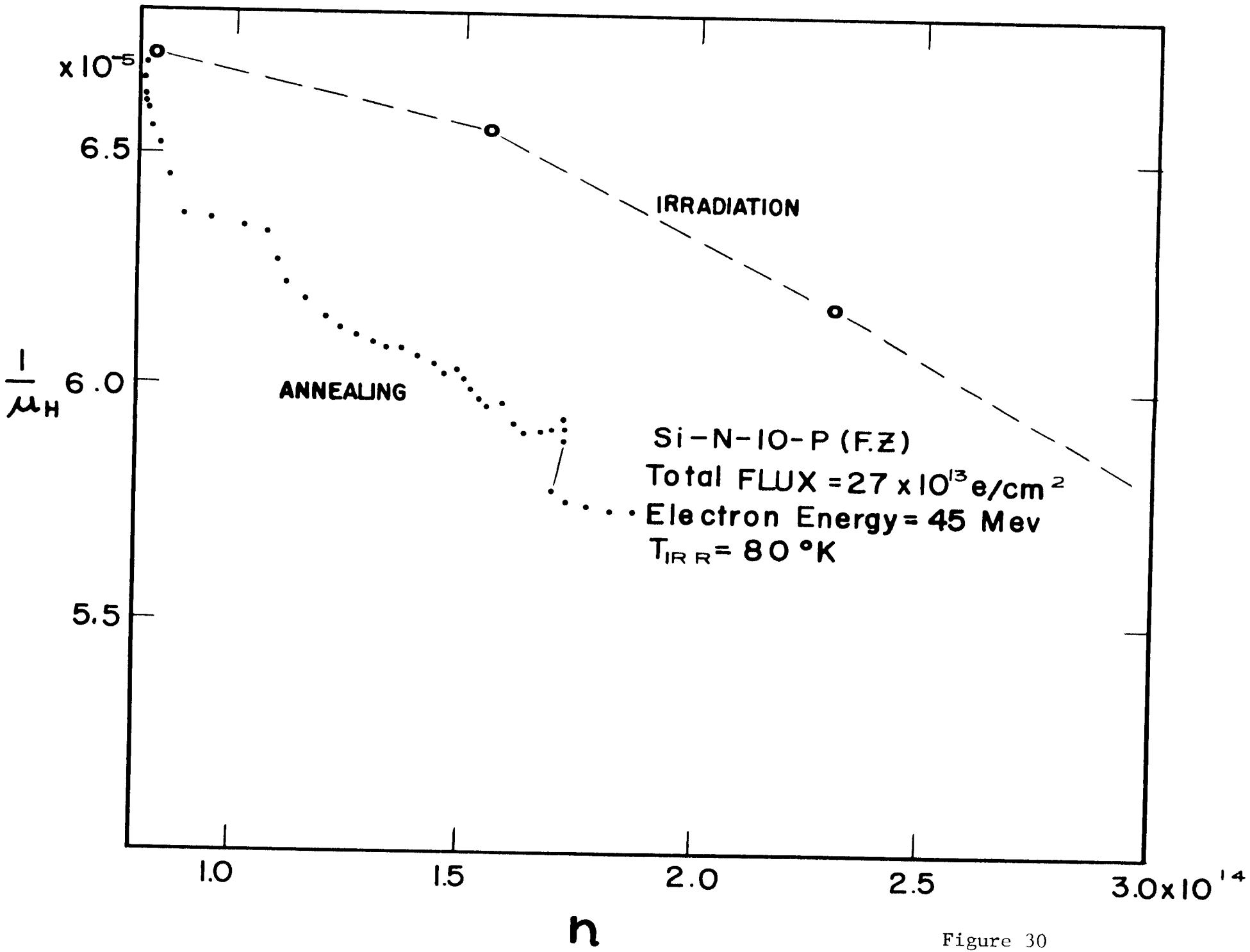
x 10⁻⁵
6.5
6.0
5.5
1/μH
IRRADIATION
ANNEALING
Si-N-10-P (F.Z)
Total FLUX = 27 x 10¹³ e/cm²
Electron Energy = 45 Mev
T IR R = 80 °K
1.0
1.5
2.0
2.5
3.0x10¹⁴
n

Figure 30

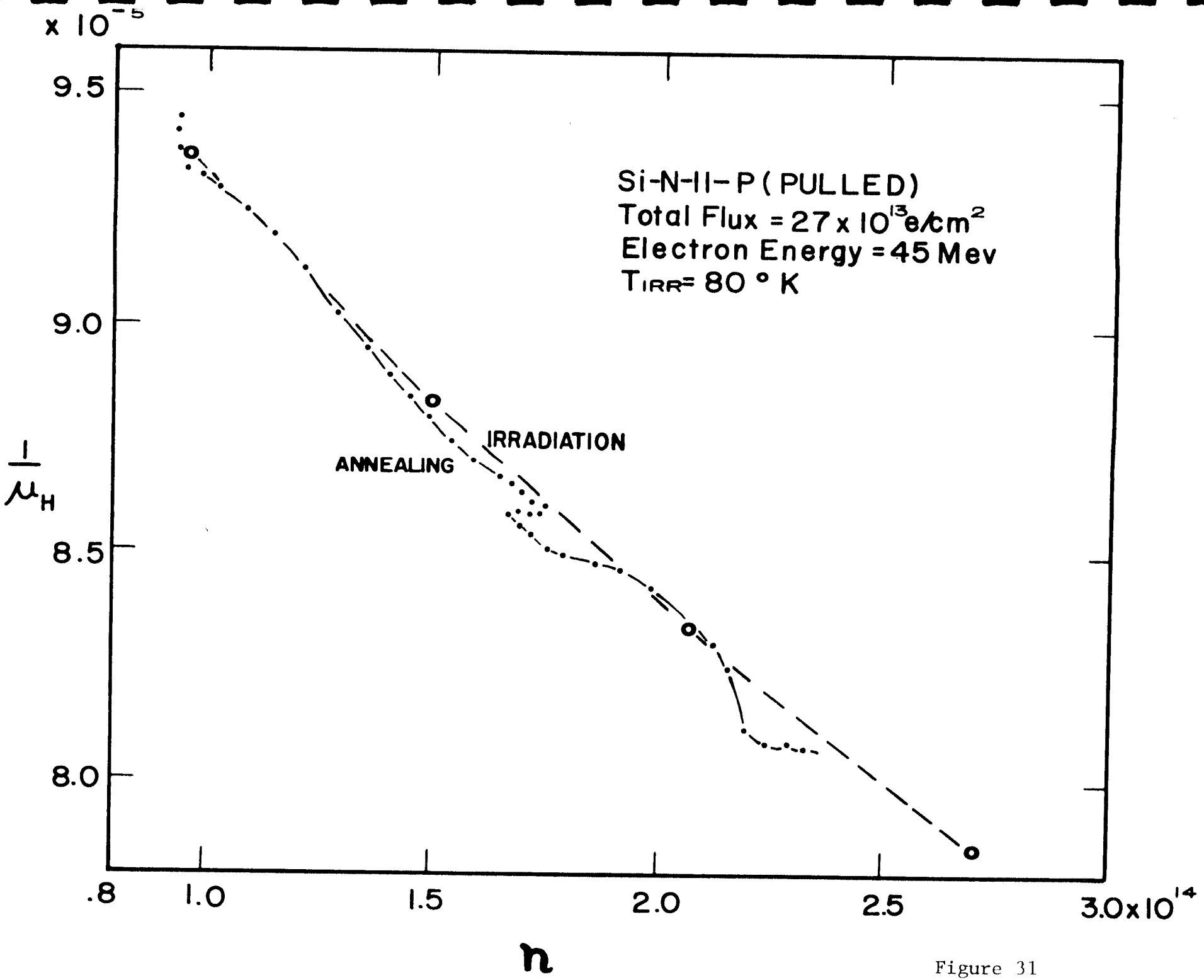
x 10⁻⁵
9.5
9.0
8.5
8.0
1/μH
Si-N-II-P (PULLED)
Total Flux = 27 x 10¹³ e/cm²
Electron Energy = 45 Mev
TIRR = 80 ° K
IRRADIATION
ANNEALING
.8
1.0
1.5
2.0
2.5
3.0x10¹⁴
n

Figure 31

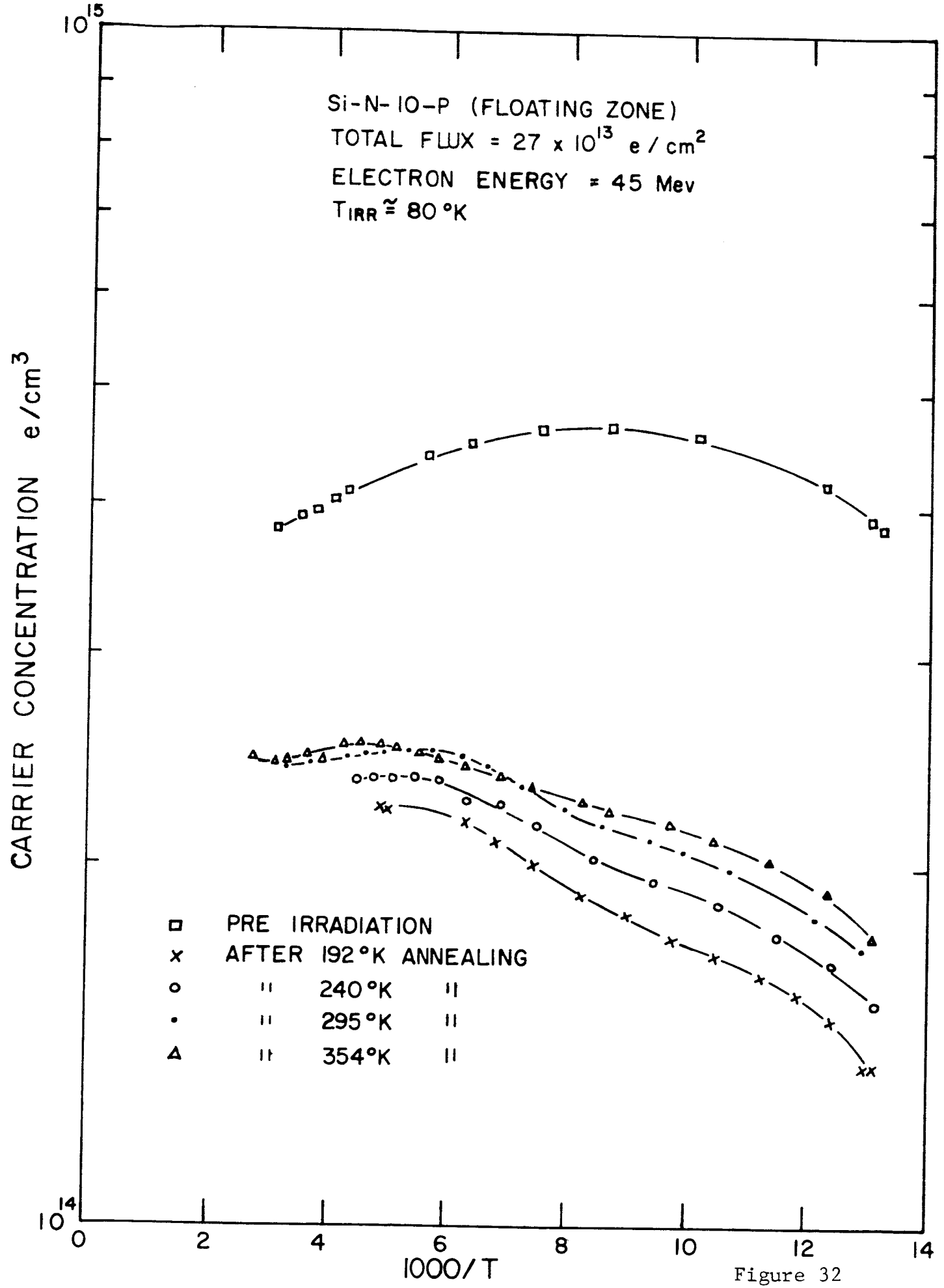
Si-N-10-P (FLOATING ZONE)
TOTAL FLUX = 27 x 10^13 e / cm^2
ELECTRON ENERGY = 45 Mev
T_IRR ≅ 80 °K
CARRIER CONCENTRATION e/cm^3
10^15
10^14
PRE IRRADIATION
AFTER 192 °K ANNEALING
" 240 °K "
" 295 °K "
" 354 °K "
0
2
4
6
8
10
12
14
1000/T

Figure 32

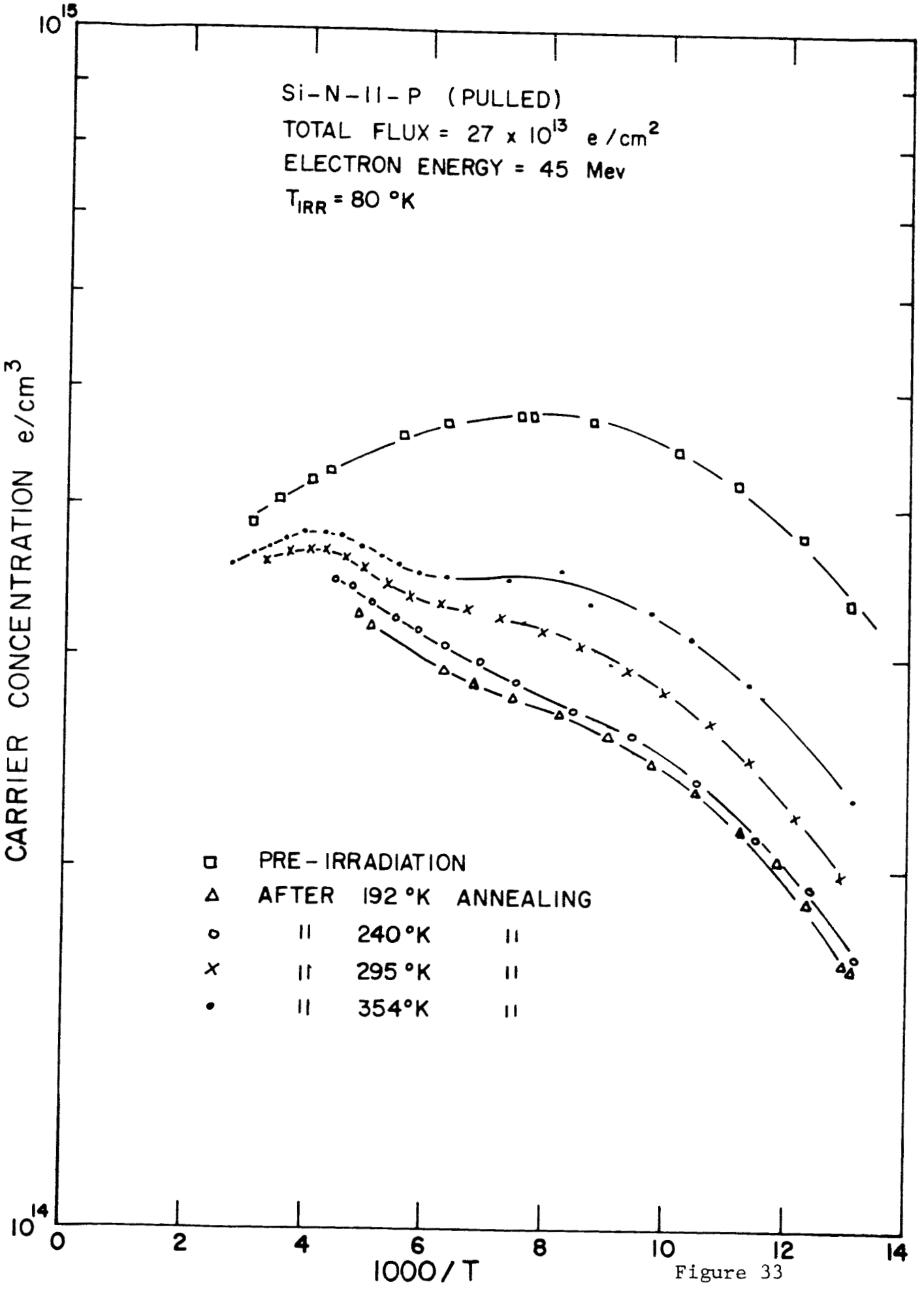
Si-N-II-P (PULLED)
TOTAL FLUX = 27 x 10^13 e/cm^2
ELECTRON ENERGY = 45 Mev
T_IRR = 80 °K
CARRIER CONCENTRATION e/cm^3
10^15
10^14
PRE-IRRADIATION
AFTER 192 °K ANNEALING
" 240 °K "
" 295 °K "
" 354 °K "
0
2
4
6
8
10
12
14
1000/T

Figure 33

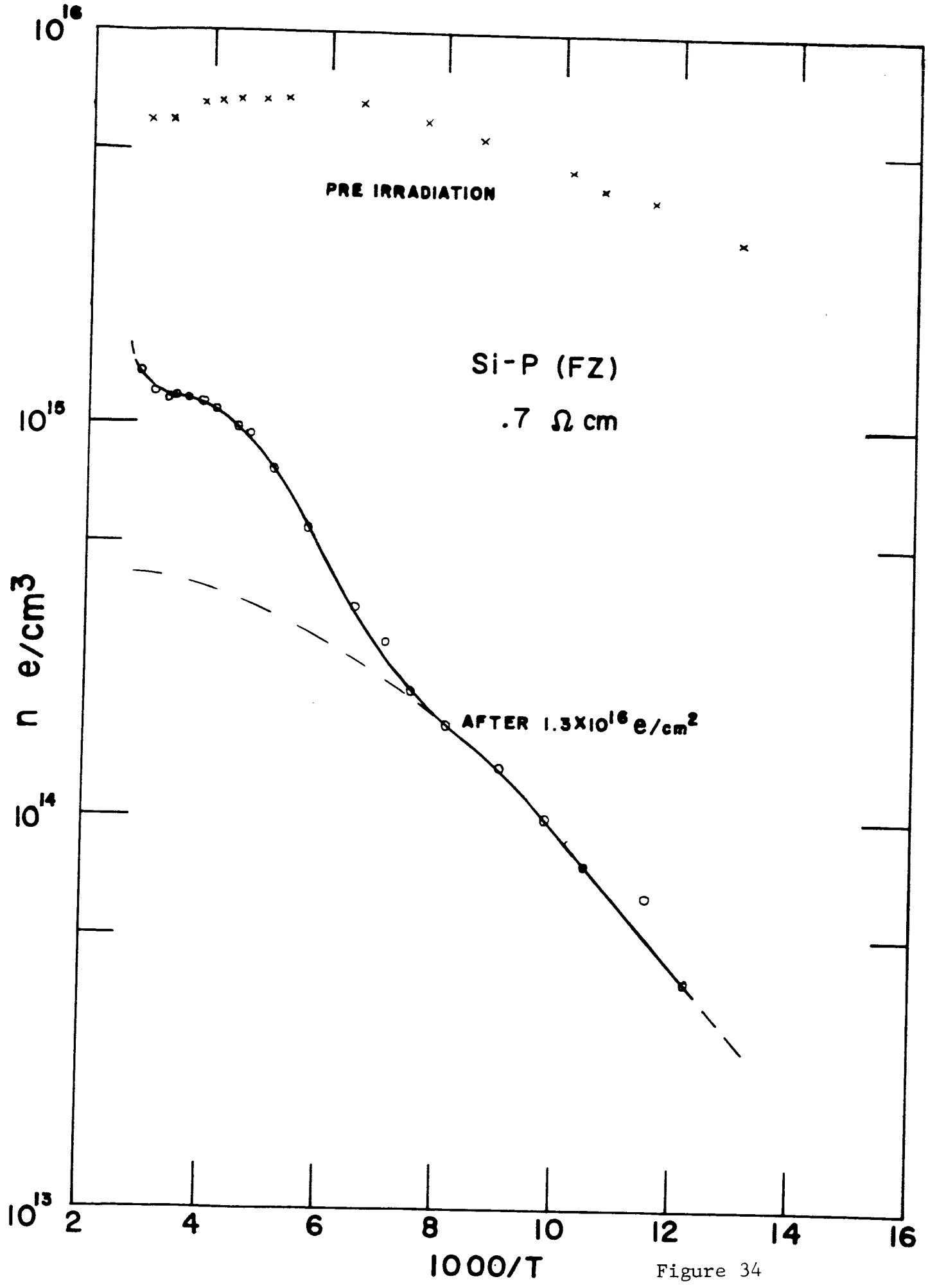
PRE IRRADIATION
Si-P (FZ)
.7 Ω cm
AFTER 1.3X10^16 e/cm^2
n e/cm^3
1000/T
10^16
10^15
10^14
10^13
2
4
6
8
10
12
14
16

Figure 34

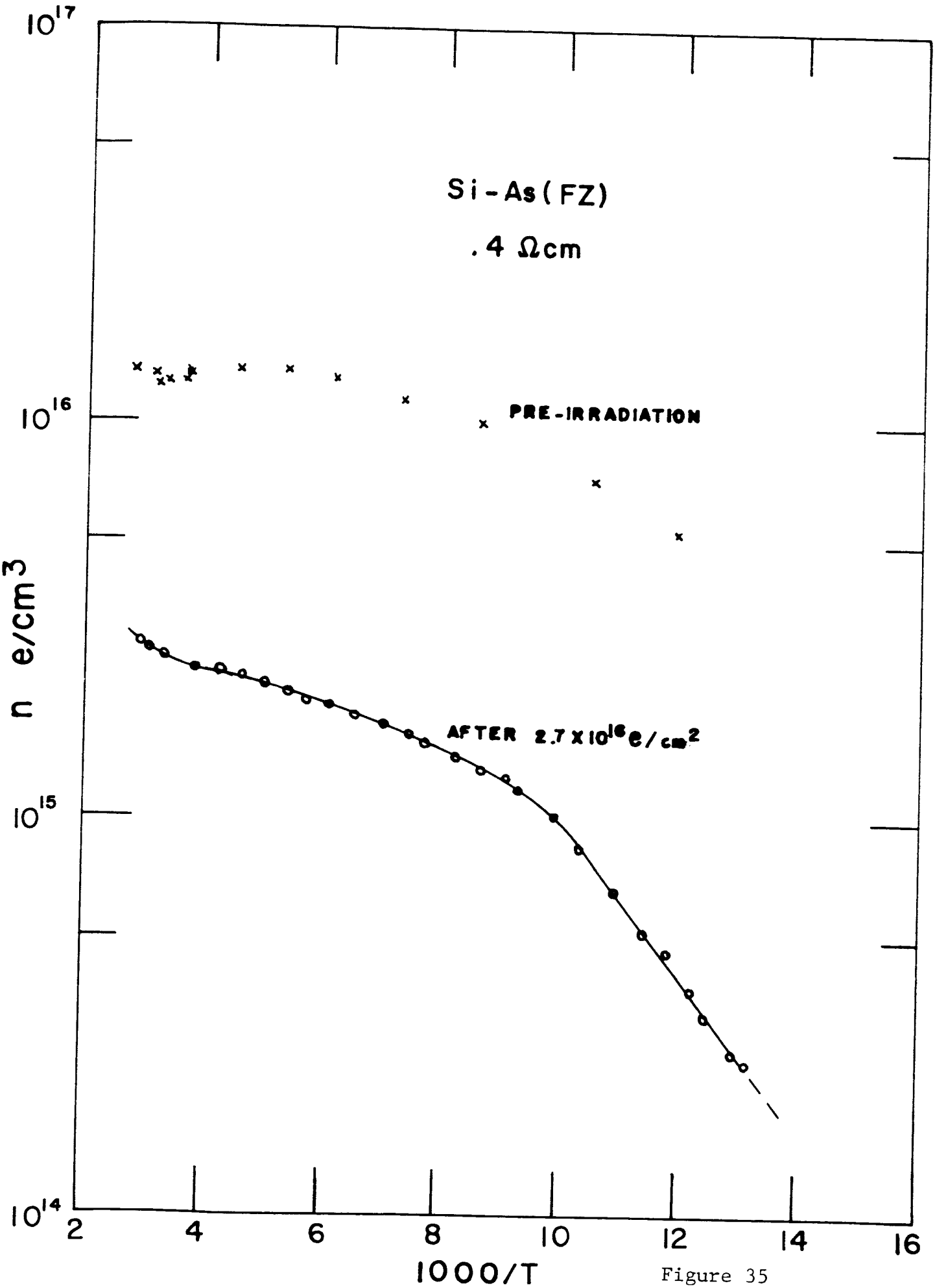
Si-As(FZ)
.4 Ωcm
PRE-IRRADIATION
AFTER 2.7 x 10^16 e/cm^2
n e/cm^3
10^17
10^16
10^15
10^14
2
4
6
8
10
12
14
16
1000/T

Figure 35

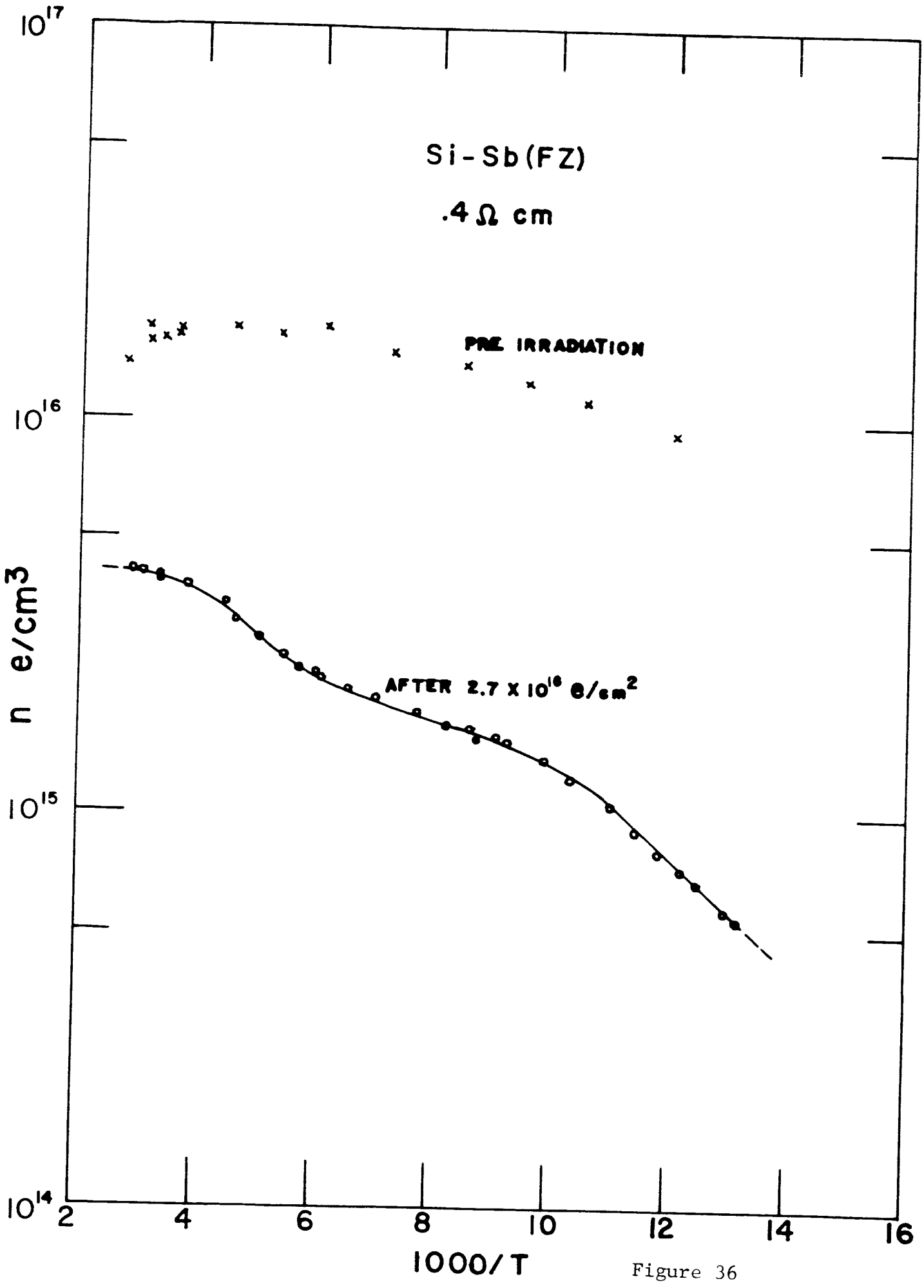
Si-Sb(FZ)
.4 Ω cm
PRE IRRADIATION
AFTER 2.7 X 10^16 e/cm^2
n e/cm3
1000/T
10^17
10^16
10^15
10^14
2
4
6
8
10
12
14
16

Figure 36

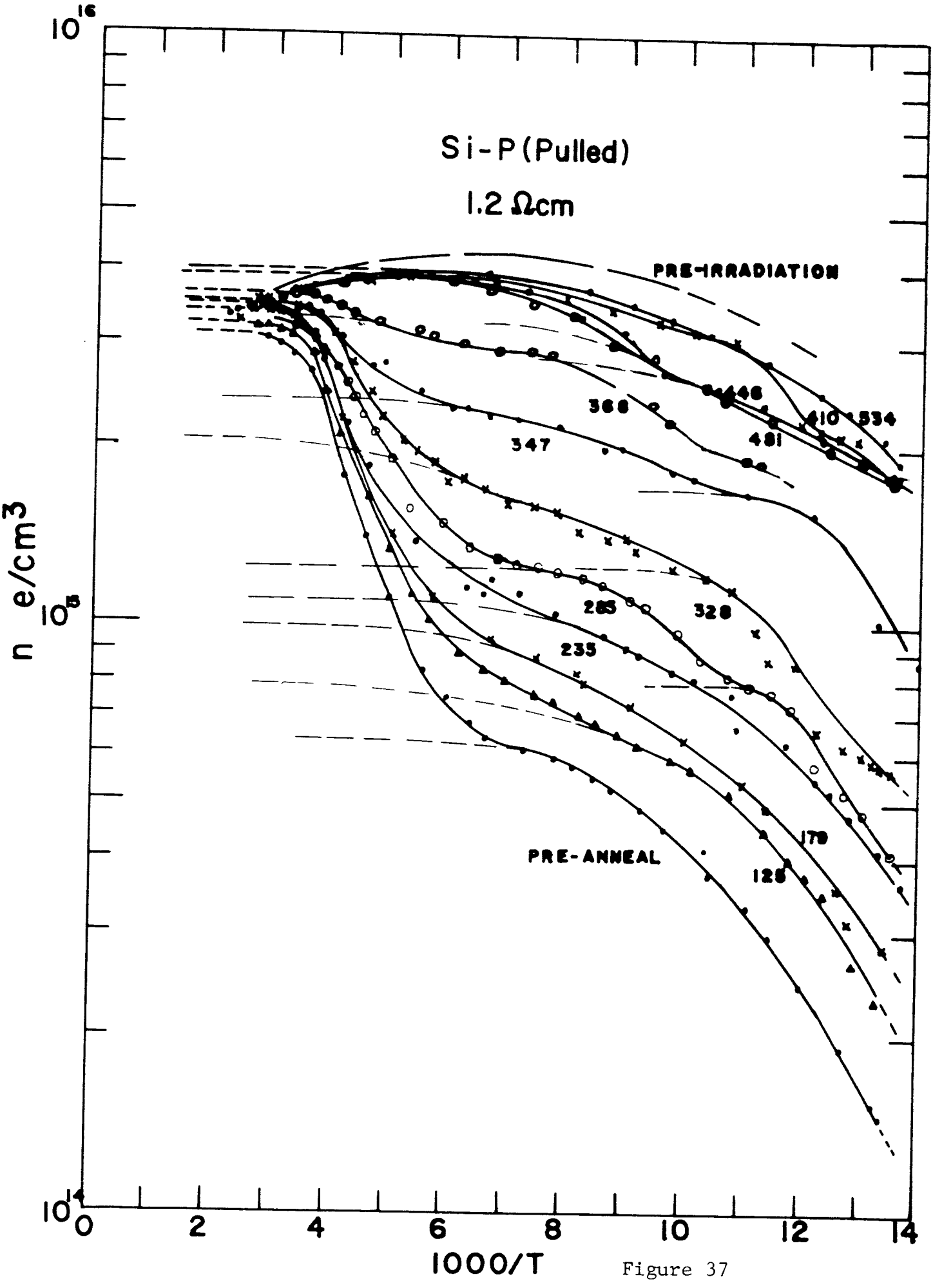
Si-P (Pulled)
1.2 Ωcm
PRE-IRRADIATION
446
388
410
534
481
347
285
328
235
179
PRE-ANNEAL
128
n e/cm3
10^16
10^15
10^14
0
2
4
6
8
10
12
14
1000/T

Figure 37

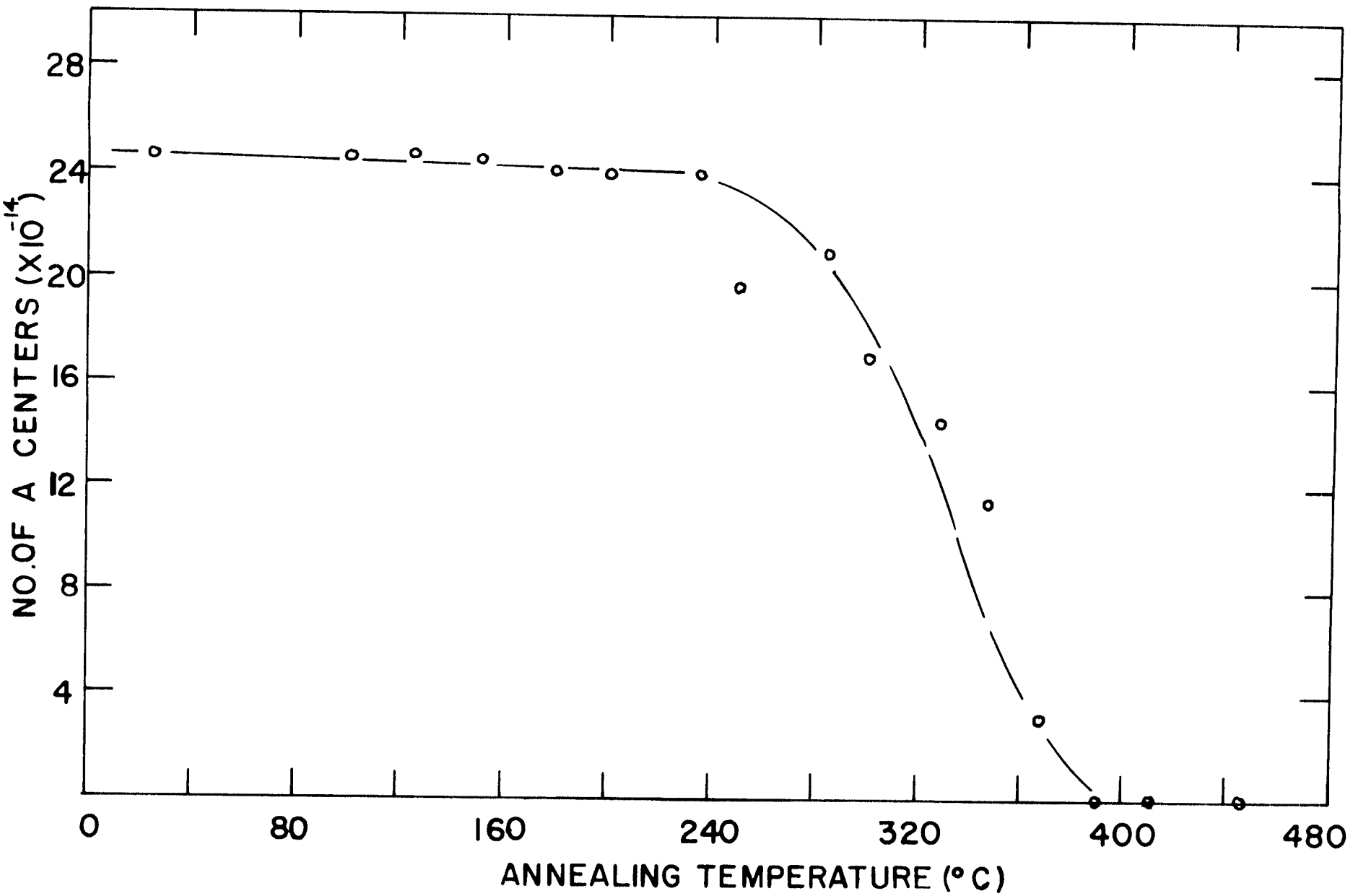
NO.OF A CENTERS (X10^{-14})
28
24
20
16
12
8
4
0
80
160
240
320
400
480
ANNEALING TEMPERATURE (°C)

Figure 38

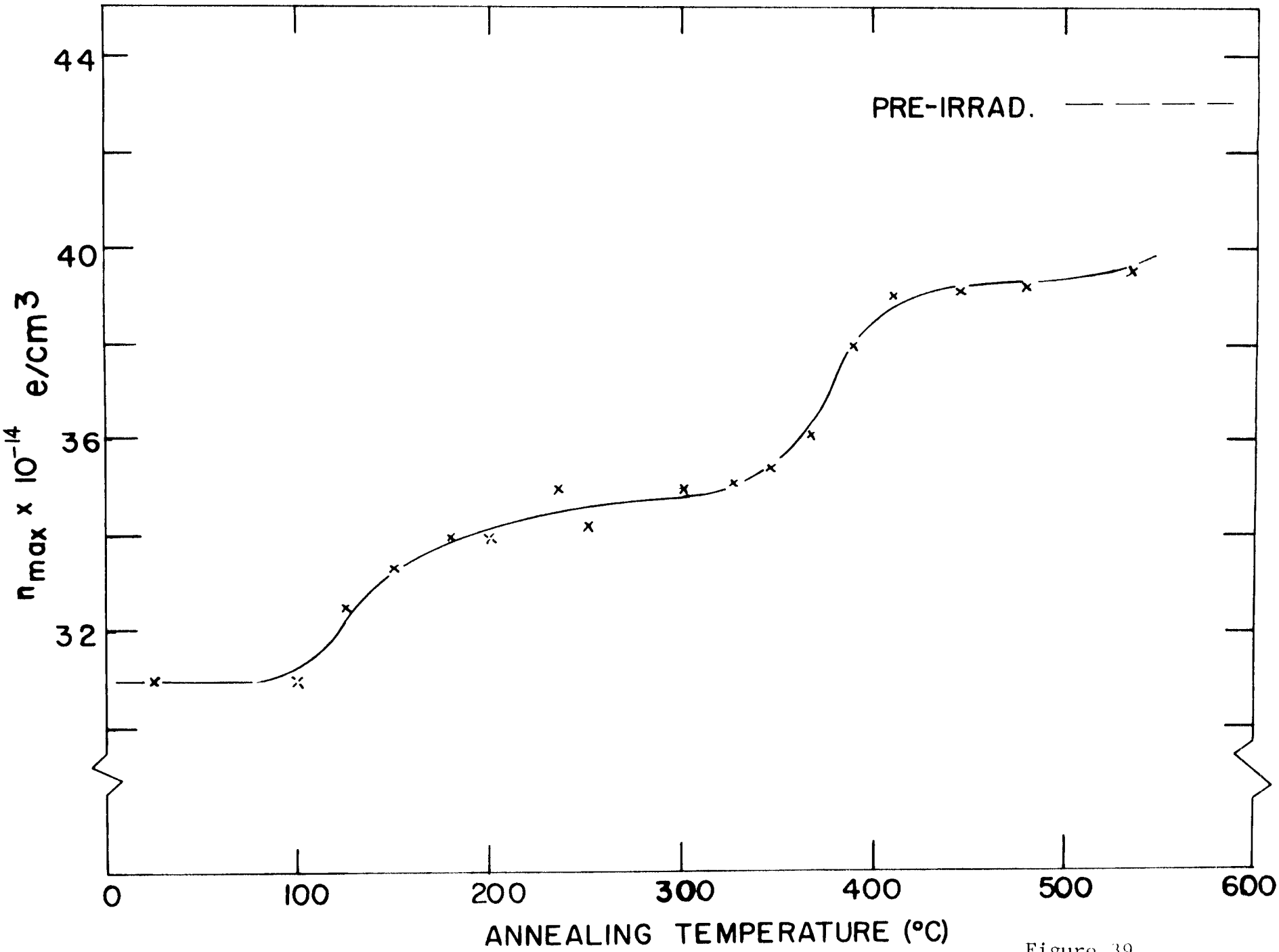
PRE-IRRAD.
44
40
36
32
$n_{max} \times 10^{-14}$ e/cm3
0
100
200
300
400
500
600
ANNEALING TEMPERATURE (°C)

Figure 39